Molecular Pharmacology Fast Forward. Published on September 13, 2016 as DOI: 10.1124/mol.116.105130
This article has not been copyedited and formatted. The final version may differ from this version.

MOL Manuscript #105130

GluN2D-containing NMDA receptors mediate synaptic transmission in hippocampal interneurons and regulate interneuron activity

Riley E. Perszyk, John O. DiRaddo, Katie L. Strong, Chian-Ming Low, Kevin K. Ogden, Alpa Khatri, Geoffrey A. Vargish, Kenneth A. Pelkey, Ludovic Tricoire, Dennis C. Liotta, Yoland Smith, Chris J. McBain, and Stephen F. Traynelis

Department of Pharmacology, Emory University School of Medicine, 1510 Clifton Road, Atlanta, Georgia 30322, United States (REP, JOD, AT, KKO, AK, SFT)
Department of Chemistry, Emory University, 1521 Dickey Drive, Atlanta, Georgia 30322, United States (JOD, KLS, DCL)
Department of Pharmacology, Yong Loo Lin School of Medicine, National University of Singapore, Singapore (CML)
Department of Anaesthesia, Yong Loo Lin School of Medicine, National University of Singapore, Singapore (CML)
Yerkes National Primate Research Center and Morris K. Udall Center of Excellence for Parkinson's Disease Research, Emory University, Atlanta, GA 30329, USA (YS)
Department of Neurology, Emory University School of Medicine, Atlanta, GA 30322, USA (YS)
Program in Developmental Neurobiology, Eunice Kennedy-Shriver National Institute of Child Health and Human Development, National Institutes of Health, Bethesda, Maryland 20892. (GAV, KAP, LT, CJM)

Molecular Pharmacology Fast Forward. Published on September 13, 2016 as DOI: 10.1124/mol.116.105130
This article has not been copyedited and formatted. The final version may differ from this version.

RUNNING TITLE PAGE

Synaptic GluN2D NMDA receptors in interneurons

Correspondence should be addressed to:

Stephen F. Traynelis
Department of Pharmacology
Emory University School of Medicine
Rollins Research Building
1510 Clifton Road
Atlanta, GA 30322
Tel 404 727 0357 Fax 404 727 0365 strayne@emory.edu

Number of Text Pages: 46

Number of Tables: 6

Number of Figures: 7

Number of References: 57

Number of Words in Abstract: 250

Number of Words in Introduction: 515

Number of Words in Discussion: 1437

Nonstandard Abbreviations:

Acetonitrile (ACN);

artificial cerebral spinal fluid (aCSF);

α-amino-3-hydroxy-5-methyl-4-isoxazolepropionic acid (AMPA);

(2R)-amino-5-phosphonovaleric acid (APV);

Molecular Pharmacology Fast Forward. Published on September 13, 2016 as DOI: 10.1124/mol.116.105130
This article has not been copyedited and formatted. The final version may differ from this version.

(3-Bromophenyl)[3,4-dihydro-6,7-dimethoxy-1-[(4-methoxyphenoxy)methyl]-2(1H)-isoquinolinyl]methanone (BIQ);

(3-Chlorophenyl)[3,4-dihydro-6,7-dimethoxy-1-[(4-methoxyphenoxy)methyl]-2(1H)-isoquinolinyl]methanone (CIQ);

complementary deoxyribonucleic acid (cDNA);

3,3' diaminobenzidine (DAB);

excitatory postsynaptic current (EPSC);

(3-Flourophenyl)[3,4-dihydro-6,7-dimethoxy-1-[(4-methoxyphenoxy)methyl]-2(1H)-isoquinolinyl]methanone (FIQ);

γ-Aminobutyric acid (GABA);

γ-Aminobutyric acid type A Receptor ($GABA_AR$);

(3-Iodophenyl)[3,4-dihydro-6,7-dimethoxy-1-[(4-methoxyphenoxy)methyl]-2(1H)-isoquinolinyl]methanone (IIQ);

inhibitory postsynaptic current (IPSC);

miniature excitatory postsynaptic currents (mEPSC);

N-methyl-D-aspartate receptors (NMDAR);

positive allosteric modulators (PAMs);

polymerase chain reaction (PCR);

reverse transcription PCR (RT-PCR);

spontaneous inhibitory postsynaptic current (sIPSC);

Molecular Pharmacology Fast Forward. Published on September 13, 2016 as DOI: 10.1124/mol.116.105130
This article has not been copyedited and formatted. The final version may differ from this version.

ABSTRACT

NMDA receptors (NMDARs) are ionotropic glutamatergic receptors that have been implicated in learning, development, and neuropathological conditions. They are typically composed of GluN1 and GluN2A-D subunits. Whereas a great deal is known about the role of GluN2A- and GluN2B-containing NMDARs, much less is known about GluN2D-containing NMDARs. Here we explore the subunit composition of synaptic NMDARs on hippocampal interneurons. GluN2D mRNA was detected by single-cell PCR and *in situ* hybridization in diverse interneuron subtypes in the CA1 region of the hippocampus. The GluN2D subunit was detectable by immunoblotting and immunohistochemistry in all subfields of the hippocampus in young and adult mice. In whole-cell patch-clamp recordings from acute hippocampal slices, (+)-CIQ, the active enantiomer of the positive allosteric modulator CIQ, significantly enhanced the amplitude of the NMDAR-component of miniature excitatory postsynaptic currents (mEPSCs) in CA1 interneurons but not pyramidal cells. (+)-CIQ had no effect in slices from *GRIN2D*-/- mice, suggesting that GluN2D-containing NMDARs participate in excitatory synaptic transmission onto hippocampal interneurons. The time course of the NMDAR-component of the mEPSC was unaffected by (+)-CIQ potentiation and was not accelerated in slices from *GRIN2D*-/- mice compared to wild type receptors, suggesting that GluN2D doesn't detectably slow the NMDAR EPSC time course at this age. (+)-CIQ increased the activity of CA1 interneurons as detected by the rate and net charge transfer of spontaneous inhibitory postsynaptic currents (sIPSCs) recorded from CA1 pyramidal cells. These data provide evidence that interneurons contain synaptic NMDARs possessing a GluN2D subunit, which can influence interneuron function and signal processing.

Molecular Pharmacology Fast Forward. Published on September 13, 2016 as DOI: 10.1124/mol.116.105130
This article has not been copyedited and formatted. The final version may differ from this version.

INTRODUCTION

NMDA receptors (NMDARs) are tetrameric assemblies comprises GluN1 subunits and GluN2 subunits. Whereas GluN3 subunits can be incorporated into NMDARs, our understanding of their role remains incomplete. Four independent genes (*GRIN2A*, *GRIN2B*, *GRIN2C*, and *GRIN2D*) encode GluN2A-D subunits, which have distinct spatial and developmental expression patterns (Traynelis 2010). Among the GluN2 subunits, little is known about the role of GluN2D in brain function, even though anatomical studies have suggested that it is expressed in many cell types, such as hippocampal interneurons (Akazawa 1994, Monyer 1994, von Engelhardt 2015). Receptor pharmacology has been studied extensively in heterologous expression systems showing incorporation of different GluN2 subunits into NMDARs confers strikingly different functional properties to the receptors, with GluN1/GluN2D receptors showing an unusually slow deactivation and low open probability (Monyer 1994, Vicini 1998, Vance 2012, Vance 2013, Wyllie 2013). Given that the deactivation time course, following removal of glutamate, controls the time course of the NMDAR-mediated component of the excitatory postsynaptic current (EPSC) (Lester 1990), the presence of GluN2D-containing receptors might alter the signal processing by changing the time course of the composite excitatory synaptic current. GluN1/GluN2D receptors also show reduced Ca^{2+} permeability and reduced Mg^{2+} sensitivity (Clarke and Johnson 2006, Retchless 2012), suggesting that inclusion of this subunit into synaptic receptors may alter synaptic signaling in multiple ways.

NMDARs have been implicated in a number of neurological processes and disorders. Accordingly, this receptor class has been the focus of intense study as a potential target for the treatment of a wide range of neurological problems including Alzheimer's disease, depression, epilepsy, Parkinson's disease, schizophrenia, and traumatic brain injury (Choi 1992, Palmer 2001, Coyle 2003, Hallett and Standaert 2004, Preskorn 2008, Coyle 2012, Preskorn 2015, Yuan 2015). Expression of different GluN2 subunits in different cells and nuclei (Akazawa 1994, Monyer 1994, Standaert 1994, Standaert 1996) may provide an opportunity to selectively target specific circuits using subunit-selective modulators. This approach should allow for enhanced efficacy and greater safety for new therapeutic strategies by restricting actions of drugs to the brain

Molecular Pharmacology Fast Forward. Published on September 13, 2016 as DOI: 10.1124/mol.116.105130
This article has not been copyedited and formatted. The final version may differ from this version.

regions and synapses involved in the pathology. While GluN2A and GluN2B receptors are expressed in principal cells, a number of studies suggest GluN2D is expressed in cortical and hippocampal interneurons (Monyer 1994, Landwehrmeyer 1995, Rudolf 1996, Thompson 2002), which should confer unique circuit properties in these regions. Here we evaluate the role of GluN2D in hippocampal interneuron function using genetic, anatomical, pharmacological, and functional experiments.

We previously described a series of GluN2C/GluN2D-selective positive allosteric modulators (PAMs) exemplified by the prototypical chiral compound CIQ (Mullasseril 2010, Santangelo Freel 2013, Santangelo Freel 2014). This pharmacological tool was recently used to evaluate subunit composition of NMDAR-mediated EPSCs onto spinal and subthalamic neurons (Hildebrand 2014, Swanger 2015). Here, we describe in detail the properties and selectivity of the active enantiomer (+)-CIQ and several closely related analogues. We subsequently use (+)-CIQ to assess the subunit composition of the synaptic NMDARs in CA1 hippocampal interneurons. Our anatomical and functional data suggest that GluN2D is expressed in hippocampal interneurons, participates in synaptic transmission, and in *ex vivo* preparations (+)-CIQ can increase the activity of these inhibitory interneurons.

Molecular Pharmacology Fast Forward. Published on September 13, 2016 as DOI: 10.1124/mol.116.105130
This article has not been copyedited and formatted. The final version may differ from this version.

MATERIALS AND METHODS

Molecular biology

All procedures using animals were reviewed and approved by the Institutional Animal Care and Use Committee of Emory University and NICHD. cDNAs for rat wild type NMDAR subunits GluN1-1a (GenBank U11418, U08261; hereafter GluN1), GluN2A (D13211), GluN2B (U11419), GluN2C (M91563), GluN2D (L31611), modified as described (Monyer 1994), GluA1 (X17184), and GluK2 (Z11548) were provided by Drs. S. Heinemann (Salk Institute), S. Nakanishi (Kyoto University), and P. Seeburg (University of Heidelberg). Plasmids containing the genes for the $GABA_A$ ($\alpha1\beta2\gamma2s$), $GABA_C$ ($\rho1$), glycine ($\alpha1$), serotonin ($5\text{-}HT_{3A}$), nicotinic acetylcholine receptor (nAChR, $\alpha1\beta1\delta\gamma$, $\alpha2\beta4$, $\alpha4\beta3$, $\alpha9\alpha10$) and purinergic (P2X2 rat, P2X2 human) receptors were provided by Drs. Heinemann (Salk), Weiss (Univ. of Texas, San Antonio), Papke (Univ. of Florida), and Hume (Univ. of Michigan). For expression in *X. laevis* oocytes, cDNA constructs were linearized by restriction endonuclease digestion, purified using the QIAquick PCR Purification Kit (Qiagen, North Rhine-Westphalia, Germany), and used as templates to transcribe cRNAs using the mMessage mMachine kit (ThermoFisher Scientific, Massachusetts, USA) following the manufacturer's protocol.

Two-electrode voltage-clamp recordings from *Xenopus laevis*

Xenopus laevis stage VI oocytes (Ecocyte Biosciences, Texas, USA) were isolated as previously described (Hansen 2013), and injected with 50 nl of water containing 5-10 ng of cRNA encoding the GluN1 and GluN2 NMDAR subunits (3:7 ratio). Oocytes were stored at 15°C in media containing (in mM) 88 NaCl, 2.4 $NaHCO_3$, 1 KCl, 0.33 $Ca(NO_3)_2$, 0.41 $CaCl_2$, 0.82 $MgSO_4$, 5 Tris-HCl (pH was adjusted to 7.4 with NaOH), 1 U/mL penicillin, 0.1 mg/mL gentamicin sulfate, and 1 μg/mL streptomycin. Two to seven days after injection, two-electrode voltage-clamp recordings were performed at room temperature. All extracellular solutions contained (in mM) 90 NaCl, 1 KCl, 10 HEPES, 0.5 $BaCl_2$, 0.01 EDTA (pH 7.4 with

Molecular Pharmacology Fast Forward. Published on September 13, 2016 as DOI: 10.1124/mol.116.105130
This article has not been copyedited and formatted. The final version may differ from this version.

NaOH). Gravity-applied solutions (4-5 ml/min) were exchanged by an 8 port Modular Valve Positioner (Hamilton Company, Nevada, USA) and controlled by custom software. Voltage and current electrodes were filled with 0.3 M and 3.0 M KCl, respectively. Oocyte currents were recorded at a holding potential of -40 mV, maintained by a two-electrode voltage-clamp amplifier (OC-725B or C, Warner Instruments, Connecticut, USA).

(+)-CIQ and related analogue stocks were prepared as a 20 mM solution in DMSO, and working solutions were prepared during rapid stirring immediately before the experiment. For concentration-response curve recordings, 1-5 mM 2-(hydroxypropyl)-β-cyclodextrin was used to increase the solubility of modulators and subsequently added to all agonist solutions to control for any direct effects. Unless indicated otherwise, current responses were elicited by application of 100 μM glutamate plus 30 μM glycine. Currents from the GluA1 and GluK2 receptors were evoked with 100 μM glutamate; oocytes expressing GluK2 were soaked in 10 μM concanavalin-A for 5 min prior to recording. Currents were evoked for the following receptors using the agonist concentrations indicated: $GABA_C$ ρ1 (2 μM GABA), $GABA_A$ α1β2γ2 (20 μM GABA), glycine α1 (50 μM glycine), 5-HT3A (15 μM serotonin), nicotinic acetylcholine α1β1δγ (20 μM acetylcholine), α4β2 (1 μM acetylcholine), α7 (100 or 300 μM acetylcholine), and the P2X2 receptor (9 μM ATP).

Electrophysiological recordings of hippocampal interneurons

Horizontal hippocampal brain slices (300 μm) were made from C57Bl/6 mice (post-natal day 7-14 or P7-14, unless otherwise stated) using a vibratome (TPI, Missouri, USA). During preparation, the slices were bathed in ice-cold (0-2°C) artificial cerebral spinal fluid (slicing-aCSF containing in mM, 75 NaCl, 2.5 KCl, 1.25 NaH_2PO_4, 25 $NaHCO_3$, 5 $MgCl_2$ or $MgSO_4$, 0.5 $CaCl_2$, 20 glucose, 70 sucrose, and bubbled with 95% O_2/5% CO_2, Supplemental Table S1). After preparation, slices were allowed to recover for 1 hour at 37°C before use in experimentation. For single-cell RT-PCR analysis of interneuron mRNA (from C57BL/6 mice P14-21), slices were transferred to a recording chamber and perfused with the RT-PCR-aCSF (containing in

Molecular Pharmacology Fast Forward. Published on September 13, 2016 as DOI: 10.1124/mol.116.105130
This article has not been copyedited and formatted. The final version may differ from this version.

mM, 130 NaCl, 24 $NaHCO_3$, 3.5 KCl, 1.25 NaH_2PO_4, 2.5 $CaCl_2$, 1.5 $MgCl_2$, 10 glucose, bubbled with 95% O_2/5% CO_2, and pH 7.4, Supplemental Table S1) and supplemented with 0.01 mM bicuculline methobromide. Recording electrodes were filled with the RT-PCR-internal solution (containing in mM, 130 K-gluconate, 10 KCl, 0.6 EGTA, 10 HEPES, 2 $MgCl_2$, 2 Na-ATP, 0.3 Na-GTP, and pH 7.2-7.3, Supplemental Table S2) and supplemented with 0.1% biocytin. Hippocampal interneurons were recorded in current-clamp mode to assay basic membrane properties and firing patterns in response to a series of square wave current injections (+/- 200 pA). At the end of the recording period the cell cytoplasm was aspirated into the recording electrode, an outside-out patch was obtained, and the pipette contents were subsequently expelled into a test tube for single-cell RT-PCR processing as described below.

Whole-cell voltage-clamp recordings of miniature EPSCs (mEPSCs) were made using the mEPSC-aCSF (containing in mM, 130 NaCl, 2.5 KCl, 1.25 NaH_2PO_4, 25 $NaHCO_3$, 0.1 $MgCl_2$ or $MgSO_4$, 2.5 $CaCl_2$, and 20 glucose, Supplemental Table S1) supplemented with 0.01mM bicuculline methobromide or gabazine and 0.5 μM tetrodotoxin (TTX). Patch recording electrodes filled with the mEPSC-internal solution (containing in mM, 110 Cs-gluconate, 30 CsCl, 5 HEPES, 4 NaCl, 0.5 $CaCl_2$, 2 $MgCl_2$, 5 BAPTA, 2 Na-ATP, 0.3 Na-GTP, Supplemental Table S2) supplemented with 1 mM QX-314 and 0.1% biocytin (pH 7.35, 285-295 mOsm). The bath temperature was maintained at 29-32°C throughout the experiment using an in-line solution heater and a bath chamber heating element (Warner Instrument Corporation, Hamden, CT, USA). Thin walled borosilicate glass (1.5 mm outer and 1.12 mm inner diameter, WPI Inc., FL, USA) was used to fabricate recording electrodes (3-5 MΩ), which were positioned using a micromanipulator (Luigs and Neumann, North Rhine-Westphalia, Germany) for whole-cell patch-clamp recording; currents were recorded using an Axopatch 1D and filtered at 1 kHz (-3 dB) digitized at 2 kHz by a Digidata 1440A for analysis off line (Molecular Devices, California, USA). To minimize uncontrolled voltage-gated receptor activation when changing the membrane holding potential during an experiment, the holding potential was slowly altered at a rate less than 4 mV/s. For experiments testing the effects of (+)-CIQ on mEPSC properties, slices were first equilibrated with aCSF supplemented with the $GABA_A$ receptor antagonist gabazine (10 μM) and

Molecular Pharmacology Fast Forward. Published on September 13, 2016 as DOI: 10.1124/mol.116.105130
This article has not been copyedited and formatted. The final version may differ from this version.

containing reduced Mg^{2+} (0.1 mM). Following equilibration, mEPSCs were recorded 3-6 minutes to determine the baseline properties. We subsequently recorded with either a vehicle solution of the same composition or a solution that contained 10 μM (+)-CIQ. (+)-CIQ solutions were made from 20 mM DMSO stock and mixed immediately before the switch in perfusion; an equivalent amount of DMSO was added to the vehicle recording solution (Figure 5A). We subsequently switched to aCSF supplemented with the competitive NMDAR-selective competitive antagonist APV (200 μM) to confirm that the slow component we recorded was mediated by NMDARs, followed by a switch to aCSF supplemented with both APV and DNQX (10 μM) to confirm that the mEPSCs we analyzed arose from AMPA receptors; no mEPSCs could be detected in the presence of DNQX. The tubing and chamber were washed with ethanol followed by extensive aCSF rinsing between recordings from each cell to remove any residual (+)-CIQ from tubing and slice-chamber.

For whole-cell patch-clamp recordings of evoked EPSCs, hippocampal slices (300-350 μm thick) were prepared from P14-21 C57BL/6 mice as previously described (Pelkey 2005, Pelkey 2006). This age was chosen to match the single cell PCR studies, which were performed at the same time. After recovery, slices were transferred to a recording chamber and perfused with the EPSC-aCSF extracellular solution (containing in mM, 130 NaCl, 24 $NaHCO_3$, 3.5 KCl, 1.25 NaH_2PO_4, 2.5 $CaCl_2$, 1.5 $MgCl_2$, 10 glucose, Supplemental Table S1) and supplemented with 0.01 mM bicuculline methobromide. Diverse interneurons throughout the hippocampus were visually identified with IR/DIC videomicroscopy and targeted for whole-cell recordings (MultiClamp 700A amplifier, Molecular Devices) in voltage-clamp mode using electrodes (3-5MΩ) pulled from borosilicate glass filled with the EPSC-internal solution (containing in mM, 100 Cs-gluconate, 5 CsCl, 0.6 EGTA, 5 BAPTA, 5 $MgCl_2$, 8 NaCl, 2 Na-ATP, 0.3 Na-GTP, 40 HEPES, Supplemental Table S2) supplemented with 0.1 mM spermine, and 1 mM QX-314 (pH 7.2-7.3, 290-300 mOsm). EPSCs were evoked at 0.2 Hz by low intensity stimulation (150 μs/10–30 μA) via a constant current isolation unit (A360, WPI Inc.) connected to a patch electrode filled with oxygenated extracellular solution. The stimulating electrode was placed within 50-100 μm of the recorded cell. Stable dual component

Molecular Pharmacology Fast Forward. Published on September 13, 2016 as DOI: 10.1124/mol.116.105130
This article has not been copyedited and formatted. The final version may differ from this version.

(AMPAR/NMDAR) synaptic responses were obtained at a holding potential of -60 mV, then slices were perfused with DNQX (20 μM), and the holding potential was changed to +50 mV to relieve Mg^{2+} block and record the pharmacologically-isolated NMDAR-component of evoked EPSCs. In some experiments, EPSCs were evoked by paired current stimulation of the Schaffer collaterals (200 ms interval) to monitor the EPSC paired-pulse ratio as a metric of presynaptic function. Data was filtered at 3.0 kHz and acquired at 20 kHz for analysis off-line with pClamp 9.0 software (Molecular Devices).

For whole-cell voltage-clamp recordings of sIPSCs, recordings were performed using the sIPSC-aCSF (containing in mM, 130 NaCl, 2.5 KCl, 1.25 NaH_2PO_4, 25 $NaHCO_3$, 1.0 $MgCl_2$, 2.0 $CaCl_2$, and 20 glucose, Supplemental Table S1) using patch recording electrodes filled with the same internal solution used for recording mEPSC (Supplemental Table S2) supplemented with 1 mM QX-314 and 0.1% biocytin (pH 7.35, 285-295 mOsm). $GABA_A$R-mediated currents were isolated by performing recordings at the reversal potential for EPSCs, which in these recording solutions was +10 mV.

Intracellular recording solutions for electrophysiology and single cell PCR experiments contained biocytin (0.1-0.2%), which allowed for anatomical reconstruction after the experiment conclusion. Biocytin-filled cells were stained with Alexa dye-conjugated avidin (Molecular Probes/Invitrogen, California, USA). Slices were fixed in 4% paraformaldehyde (PFA) in PBS for 12-60 hours at 4°C, and then rinsed twice with PBS and maintained in PBS until further processing. Slices were re-sectioned, mounted on slides, and imaged as previously reported (Matta 2013). Neurons were classified by their cell body localization as well as dendritic and axonal arborization.

Miniature EPSC detection and analysis

Minianalysis (Synaptosoft, Georgia, USA) was used to detect mEPSCs using amplitude and integral threshold cut-offs. Recordings were filtered using a 250 Hz low pass Butterworth filter only for detection purposes. For the detection of composite AMPAR/NMDAR-mediated currents while holding the membrane voltage at -60 mV, an amplitude threshold from 8-12 pA and an area of 40 fC were used to identify mEPSCs,

Molecular Pharmacology Fast Forward. Published on September 13, 2016 as DOI: 10.1124/mol.116.105130
This article has not been copyedited and formatted. The final version may differ from this version.

which were aligned on the time of the peak of the response. Amplitude threshold was selected based on the variance (>3 times the standard deviation of a stretch of recording with no mEPSCs) of the control recording in each experiment. An amplitude threshold of 8 pA and an area of 80 fC were used to detect NMDAR-mediated spontaneous synaptic currents at a holding voltage at +40 mV. The same detection parameters were used throughout analysis of each data set from every experiment. Each detected current was evaluated for synaptic-like shape (rapid 10-90 rise < 2 ms, an exponential decay) and rejected if there was a second mEPSC or any non-synaptic recording artifact present during the mEPSC. Following detection of mEPSCs, the original recorded mEPSC (digitized at 2 kHz) was aligned on the rising phase of the response and the time course averaged. The experimenter was blinded to the identity of the recording group while sorting mEPSCs. mEPSCs selected for inclusion were further analyzed using custom written Matlab scripts to determine mEPSC peak amplitude, decay time constants, the amplitude of the NMDAR-component of the mEPSC. The deactivation time course for the rapid (AMPAR) and slower (NMDAR) components of the mEPSC were evaluated by non-linear least-squares fitting of a dual exponential equation to the synaptic waveform as follows:

$$I = Amplitude_{\mathrm{FAST}}\, e^{\left(\frac{time}{-\tau_{\mathrm{FAST}}}\right)} + Amplitude_{\mathrm{SLOW}}\, e^{\left(\frac{time}{-\tau_{\mathrm{SLOW}}}\right)}$$

where I is the current response, $Amplitude_{\mathrm{FAST}}$ is the amplitude of the fast component, *time* is the time of the response in reference to the peak response amplitude, τ_{FAST} is the deactivation time constant of the fast component, $Amplitude_{\mathrm{SLOW}}$ is the amplitude of the slow component, and τ_{SLOW} is the deactivation time constant of the slow component. In mEPSC recordings, τ_{FAST} was assumed to reflect the AMPAR-component, and determined by fitting the response in the presence of the competitive NMDAR antagonists APV. To estimate the amplitude of the NMDAR-mediated component of EPSC, the mean current between 40-50 ms after the peak of the AMPAR response was measured. The AMPAR/NMDAR ratio was calculated by dividing $Amplitude_{\mathrm{FAST}}$ by $Amplitude_{\mathrm{SLOW}}$.

Molecular Pharmacology Fast Forward. Published on September 13, 2016 as DOI: 10.1124/mol.116.105130
This article has not been copyedited and formatted. The final version may differ from this version.

The NMDAR-mediated evoked EPSC peak amplitude was measured within a 2 ms window around the peak of the waveform obtained from the average of 30-40 individual EPSCs. Rise time was determined as the time for the current to rise from 20 to 80% of the peak amplitude. The EPSC time course was analyzed by fitting a single exponential component to the averaged waveform between 90% and 20% of the peak amplitude. For these experiments, EPSC decay kinetics were measured using the second EPSC waveform evoked by the paired stimuli and the paired-pulse ratio was calculated as P2/P1, where P1 represents the amplitude of the first evoked current and P2 the amplitude of the second synaptic current measured from the averaged EPSC waveform.

Spontaneous IPSCs (sIPSCs) were detected using Minianalysis as described above, with an amplitude threshold of 6-8 pA and an area of 30 fC at a holding potential of +10 mV. sIPSC recordings were analyzed for their relative frequency throughout the experiment. A rolling average (60 second window) of the sIPSC frequency was normalized to a 60 second period in pre-treatment control phase of experiment for each cell and the resulting plots averaged between cells to produce the composite response for all recordings in an experimental group. The comparable 60 second periods in the baseline and at the end of the application of (+)-CIQ phases was used to determine the change in sIPSC frequency and amplitude. To determine the integral of the spontaneous activity, the mean current in a stretch of the recording free of sIPSCs was subtracted from the full record. The current response in a 50 second window was integrated during the baseline, at the end of the (+)-CIQ phases, and in the presence of gabazine. The gabazine current was subtracted from baseline and (+)-CIQ and the ratio presented.

Single-cell reverse transcription-PCR

Reverse transcription (RT) was performed on the interneuron cytoplasm harvested as described above. Reactions were run in a final volume of 10 µL as described previously (Lambolez 1992), and two series of PCR were performed as described previously (Cauli 1997). The cDNAs present in 10 µl of the RT reaction first were amplified simultaneously using primer pairs with the sense and antisense primers

Molecular Pharmacology Fast Forward. Published on September 13, 2016 as DOI: 10.1124/mol.116.105130
This article has not been copyedited and formatted. The final version may differ from this version.

positioned on 2 different exons (see Supplemental Table S3). Taq polymerase (2.5 U; Qiagen) and 20 pmol of each primer were added to the buffer supplied by the manufacturer (final volume, 100 µl), and 21 cycles (94°C for 30 s, 60°C for 30 s, and 72°C for 30 s) of PCR were run. Second rounds of PCR were performed using 2 µl of the first PCR product as template. In this second round, each cDNA was amplified individually with a second set of primers internal to the primer pair used in the first PCR, and positioned on 2 different exons (see nested primer pairs in Supplemental Table S3). Thirty-five PCR cycles were performed with cycle temperatures/times as described above. 10 µL of each individual PCR were run on a 2% agarose gel, with ΦX174 digested by HaeIII as a molecular weight marker; gels were stained with ethidium bromide and analyzed. The RT-PCR protocol was tested on 100 ng of total RNA purified from mouse whole brain. All the transcripts were detected from 100 ng of whole-brain RNA. The sizes of the PCR-generated fragments were as predicted by the mRNA sequences (see Supplemental Table S3).

In situ hybridization

Two C57Bl/6 mice aged P25 were used for *in situ* hybridization. Animals were anesthetized with isoflurane. Brains were then removed and flash frozen in liquid N_2. Frozen brains were cut into 12 µm coronal sections using a cryostat (Leica, Buffalo Grove, IL, USA) and were mounted on slides. Slide mounted sections were fixed in 4% PFA and dehydrated in increasing concentrations of ethanol. Hybridization and amplification steps were then performed, in a similar fashion as (Pelkey 2015), using RNAscope Flourescent Multiplex kit (Advanced Cell Diagnostics Inc., Hayward, CA). Probes used include *GRIN2D* (cat no. 425951), parvalbumin (PV, cat no. 421931), cannabinoid receptor type 1 (CB1R, cat no. 420721), somatostatin (SOM, cat no. 404631).

Hippocampal field tissue preparation and western blotting for GluN2D

Molecular Pharmacology Fast Forward. Published on September 13, 2016 as DOI: 10.1124/mol.116.105130
This article has not been copyedited and formatted. The final version may differ from this version.

Wild type C57Bl/6 P9, P17, P30, P58 and P74 mice (both male and female, 3 in each age group) were used for western blot analysis of GluN2D expression. Experiments included analysis of three *GRIN2D*-/- mice at P9. Animals were euthanized by isoflurane overdose, the brains rapidly were removed, and 500 µm slices were cut in ice-cold PBS on a vibratome (TPI, Missouri, USA). The whole hippocampus was dissected out for some slices and tissue punches of the CA1 region, the CA3 region, and the dentate gyrus/hilar region collected using a 0.75 mm Stoelting tissue punch from other slices. The tissue was frozen on dry ice, and subsequently homogenized in lysis buffer containing (in mM) 150 NaCl, 50 Tris, 50 NaF, 5 EDTA, 5 EGTA, 1% Triton, 1% SDS, and protease inhibitors (cat. number 88266, Pierce, Thermo Scientific) at pH 7.4. A Bradford assay was used to quantify and normalize total protein concentrations, and the samples were then mixed with 4x Laemmli buffer (containing 40% glycerol, 240 mM Tris/HCl pH 6.8, 8% SDS, 0.04% bromophenol blue, 175 mM DDT). After samples were heated to 95°C for 5 min, they were separated by electrophoresis using a 4-20% SDS-PAGE gel, and transferred to a PVDF membrane (cat. number 162-0177, Bio-Rad). The mouse anti-GluN2D (Millipore, MAB5578, 1:5000), mouse anti-tubulin (Sigma-Aldrich, 1:50,000), and horseradish peroxidase-conjugated goat anti-mouse (Jackson Immunoresearch, 1:10,000) antibodies were used. Between probing for different primary antibodies, Restore Stripping Buffer (Pierce) was applied for 10 min to strip off previous probe. Band intensities were imaged (Bio-Rad Gel Doc XR+ Imager, cat. number 1708195) from films exposed to chemiluminescence signals, and band intensity was analyzed using ImageJ.

Off-Target Screening using the Psychoactive Drug Screening Program

The National Institute of Mental Health Psychoactive Drug Screening Program (PDSP, http://pdsp.med.unc.edu/) evaluated the potential off-target effects of (+)-CIQ and (-)-CIQ (Besnard 2012). A total of 45 targets were assayed, including the serotonin receptor 5-HT1A, 5-HT1B, 5-HT1D, 5-HT1E, 5-HT2A, 5-HT2B, 5-HT2C, 5-HT3, 5-HT5A, 5-HT6, 5-HT7, adrenergic receptor α1A, α1B, α1D, α2A, α2B, α2C, β1, β2, β3, benzodiazepine site in rat brain, dopamine receptor D1, D2, D3, D4, D5, opioid receptor δ,

Molecular Pharmacology Fast Forward. Published on September 13, 2016 as DOI: 10.1124/mol.116.105130
This article has not been copyedited and formatted. The final version may differ from this version.

κ, μ, histamine receptor H1, H2 , H3, H4, muscarinic receptor M1, M2, M3, M4, M5, sigma receptor 1, 2, peripheral benzodiazepine receptor (PBR), norepinephrine transporter, dopamine transporter, serotonin transporter, and GABA type-A receptor. A fixed concentration assay was used to determine if a radioligand for each receptor could be displaced by each test compound. If it was determined that more than 50% of the radioligand was displaced, a secondary assay was run to determine the affinity of this interaction. This assay was designed to determine the affinity of the test compound at the potential target when *Ki* was less than 10 μM.

Chemistry methods

Racemic mixtures of CIQ (Life Chemicals, F0535-0139, Ontario, Canada), FIQ (Life Chemicals, F0535-0142), IIQ (synthesized as described in Santangelo Freel et al 2013, and BIQ (Life Chemicals, F0535-0181) were separated via a ChiralPak OD-RH reverse phase 30 mm x 250 mm, 5 μM column utilizing ACN (0.1% formic acid) and H_2O (0.1% formic acid) as the solvent system, and the conditions for each compound are listed in Table 1. The enantiomeric excess was calculated for all enantiomer pairs as 100% ee using an Agilent 1200 HPLC pump on a Chiral OD-RH column (4.6 mm x 150 mm, 5 μm) utilizing ACN (0.1% formic acid) and H_2O (0.1% formic acid) as the solvent system; the conditions are given in Table 2. All retention times for the ChiralPak and analytical chiral OD-RH along with optical rotation values are listed in Table 2. Optical rotation values were obtained using a polarimeter. Purity of both enantiomers was established to be greater than 95% by HPLC.

Statistical analysis

Non-linear least squares fitting was performed on experimental data from individual concentration-response curves from each oocyte, which were fitted by the Hill equation:

$$\frac{I}{I_{[A]=0}} = (Pot_{max} - 1)\left(\frac{[A]^h}{[A]^h + {EC_{50}}^h}\right) + 1$$

Molecular Pharmacology Fast Forward. Published on September 13, 2016 as DOI: 10.1124/mol.116.105130
This article has not been copyedited and formatted. The final version may differ from this version.

where I is the current response, Pot_{max} is the maximal predicted potentiation of the glutamate/glycine response (and expressed as a percent for clarity), [A] is the concentration of the modulator, h is the Hill slope, and EC_{50} is the half-maximally effective concentration of the modulator. The potentiated current response was expressed as percent of control. Displayed fitted curves were obtained by fitting all oocyte data from each compound concentration condition.

Data are shown as mean ± SEM unless otherwise indicated. Experimental sample size was chosen to ensure a power level of at least 0.80 when detecting effect size changes ranging from 30-50%. Data were evaluated for statistical significance using a one-way ANOVA with Dunnett's multiple comparison test with α set to 0.05 or a paired t–test, as appropriate. For statistical testing of EC_{50} values, a one-way ANOVA with Dunnett's multiple comparison test was calculated using the logarithm of the EC_{50} values with α set to 0.05.

Molecular Pharmacology Fast Forward. Published on September 13, 2016 as DOI: 10.1124/mol.116.105130
This article has not been copyedited and formatted. The final version may differ from this version.

RESULTS

Enantiomeric preference of a series of GluN2C/D-selective NMDAR positive allosteric modulators

To explore the subunit composition of the NMDARs underlying EPSCs in CA1 interneurons, we utilized a series of GluN2C/GluN2D-selective allosteric modulators (Mullasseril 2010, Santangelo Freel 2013). Racemic CIQ was described as the first GluN2C and GluN2D subunit-selective positive allosteric modulator for NMDARs (Mullasseril 2010), with virtually all activity residing in the (+) enantiomer (Santangelo Freel 2013). Although the stereochemistry of the two enantiomers has not been absolutely resolved, a model of the stereoselective reduction during the chiral synthesis of the enantiomers predicts that the (+)-enantiomer is the (R)-enantiomer (Santangelo Freel 2014). In the absence of a crystal structure of either enantiomer, however, we will refer to the active enantiomer as (+)-CIQ (Figure 1B).

We first evaluated the properties of purified (+)-CIQ as well as closely related halogen-substituted analogues of CIQ (Table 3). In agreement with previous work using (±)-CIQ, neither (+)-CIQ nor (-)-CIQ affected responses of GluN1/GluN2A or GluN1/GluN2B diheteromeric NMDARs expressed in *Xenopus laevis* oocytes when activated by 100 μM glutamate and 30 μM glycine (Figure 1C and D, Table 3). (+)-CIQ enhanced the response of GluN1/GluN2C and GluN1/GluN2D NMDARs activated by maximally effective co-agonist concentrations, whereas (-)-CIQ had minimal effects at these NMDARs (Figure 1E, and F, Table 3). To further examine the enantiomeric specificity of this class of modulator, other enantiopure halogenated isoquinolines (FIQ, BIQ, IIQ) were assayed for their activity on recombinant GluN1/GluN2 diheteromeric NMDARs. In all cases, activity resided with the (+) enantiomers (Table 3).

A previous evaluation of potential off-target activity of racemic CIQ suggested it was highly selective (Santangelo Freel 2013), with a few notable exceptions, such as low μM actions on 5-HT6 serotonin receptor, peripheral benzodiazepine receptor (PBR), and several nACh receptors. Off target analysis of 45 assayed receptors (see *Methods*, Besnard 2012) showed that 3 μM (+)-CIQ displaced bound ligand of the serotonin 5-HT1A receptor and PBR in the initial screening assay, prompting further evaluation of affinity. The K_i of (+)-CIQ was determined to be greater than 10 μM (which was the upper boundary for this assay)

Molecular Pharmacology Fast Forward. Published on September 13, 2016 as DOI: 10.1124/mol.116.105130
This article has not been copyedited and formatted. The final version may differ from this version.

for the 5-HT1A receptor and 1.8 μM for the PBR receptor by the secondary assay. Additionally, 3 μM (-)-CIQ was found to displace bound ligand for serotonin 5-HT6, 5-HT7, and PBR receptors. Further evaluation determined that the K_i of (-)-CIQ was 1.0 μM for the 5-HT6 receptor, and greater than 10 μM for both the 5-HT7 receptor and the PBR. (+)-CIQ and (-)-CIQ were also screened at a higher concentration (20 μM) on a series of ionotropic receptors expressed in *Xenopus laevis* oocytes using two electrode voltage clamp (Figure 1G). Both (+)-CIQ or (-)-CIQ similarly inhibited nicotinic α1β1γδ acetylcholine receptors (42 ± 0.8% of control by (+)-CIQ *vs* 57 ± 17% by (-)-CIQ, unpaired t-test, p=0.54) and nicotinic α4β2 acetylcholine receptors (44 ± 5.1% by (+)-CIQ vs 34 ± 4.8% by (-)-CIQ, unpaired t-test, p=0.22), but did not significantly affect the other receptors tested. Due to reduced off-target activity, (+)-CIQ is a better tool compound than racemic CIQ for evaluation of GluN2C- and GluN2D-containing receptors.

GRIN2D mRNA and the GluN2D protein are expressed in hippocampal interneurons

Several studies suggest that cortical and hippocampal interneurons express *GRIN2D* mRNA (Monyer 1994, Rudolf 1996, Porter 1998, Cauli 2000), which encodes the GluN2D subunit. To provide more detailed information regarding interneuron subtype and NMDAR subunit expression patterns in the hippocampus, we performed single cell RT-PCR from various interneurons throughout the hippocampal formation. A total of 37 interneurons were recorded using whole-cell patch-clamp methods under current-clamp and classified by their spiking activity before harvesting their cytoplasmic contents for the analysis of mRNA (Figure 2A-C). Patched cells were filled with biocytin, allowing for *post hoc* determination of soma and axon location (Figure 2A). Single cell RT-PCR (Figure 2C) detected *GRIN2D* in multiple interneuron subpopulations of the hippocampus, including dendritic targeting bistratified and oriens-lacunosum molecular cells as well as fast spiking (parvalbumin) and regular spiking (cholecystokinin) perisomatic targeting basket cells. The location and prevalence of NMDAR subunits for the 37 interneurons assayed are summarized in Table 4 (complete cellular results are shown in Supplemental Table S4). Overall, amplified signals for *GRIN1*, *GRIN2A*, and *GRIN2B* were detected in most cells (33, 26, and 31 out of 37 interneurons, respectively).

Molecular Pharmacology Fast Forward. Published on September 13, 2016 as DOI: 10.1124/mol.116.105130
This article has not been copyedited and formatted. The final version may differ from this version.

GRIN2C was only detected in 1 of the 37 interneurons. *GRIN2D* was detected in 29 of 37 cytoplasmic harvests from randomly recorded hippocampal interneurons.

To further investigate the cell-type specificity of *GRIN2D* subunit expression, we performed fluorescent *in situ* hybridization examining mRNA expression for *GRIN2D* and interneuron-specific molecular markers. Corroborating single-cell RT-PCR data, we found *GRIN2D* in cells positive for parvalbumin (PV), cannabinoid receptor type 1 (CB1R, a marker for cholecystokinin-expressing interneurons), and somatostatin (SOM, Figure 2D-F).

As an independent assessment of GluN2D expression at the protein level, we performed immunohistochemistry on adult mouse brain sections from mice using a GluN2C/D polyclonal antibody (Supplemental Figure S1A, C). Several reports suggest that expression of GluN2D decreases throughout development (Akazawa 1994, Monyer 1994). We thus used adult animals to test whether GluN2D protein persists at older ages. Diffuse neuropil staining was evident throughout the hippocampus, in addition to staining of cell bodies. Parallel experiments showed that staining was greatly diminished in these same regions in age-matched *GRIN2D*-/- mice (Supplemental Figure S1B), confirming the specificity of the immunoreactivity for the GluN2D subunit. These data suggest that the immunostaining observed in these neurons reflected primarily GluN2D rather than GluN2C, consistent with lack of detection of *GRIN2C* in RT-PCR analysis of interneuron mRNA.

To assess the protein expression of the GluN2D subunit across hippocampal regions and through early developmental periods, we collected whole hippocampal slices (Figure 3A, B, D) from acute mouse hippocampal slices (Figure 3C, E). The expression of GluN2D was not detected in P9 *GRIN2D*-/- hippocampal preparations (Figure 3C). To assess the expression of the GluN2D subunit in the different subfields of the adult hippocampus, micropunches of tissue were isolated from slices prepared from P74 mice (Figure 3B). The GluN2D subunit was detected in all regions, with lower levels in the CA1 as compared to the dentate gyrus (Figure 3B, D). Similarly to previous studies, GluN2D is expressed in the

Molecular Pharmacology Fast Forward. Published on September 13, 2016 as DOI: 10.1124/mol.116.105130
This article has not been copyedited and formatted. The final version may differ from this version.

hippocampus of young and adult rodents but decreases in adulthood (Akazawa 1994, Monyer 1994, von Engelhardt 2015).

The NMDAR-component of mEPSCs in hippocampal interneurons is potentiated by (+)-CIQ

To investigate the subunit composition of synaptic NMDARs in interneurons, we recorded from hippocampal interneurons in the CA1 stratum radiatum under voltage clamp (V_{hold} -60 mV) using the whole-cell patch-clamp method (Figure 4A). We chose animals aged P7-14 as these ages preceded a switch from GluN2B to GluN2A (Akazawa 1994, Monyer 1994, Edman 2012, McKay 2012); these ages were also similar to those used in a recent study of NMDAR expression in hippocampal neurons (von Engelhardt 2015). Slices were bathed in aCSF supplemented with 0.5 µM TTX, 10 µM gabazine or bicuculline, and extracellular Mg^{2+} reduced to 0.1 mM to record miniature EPSCs (mEPSCs). These inward currents had a rapid rise time and a dual exponential decay thought to reflect spontaneous release of a single vesicle of glutamate (Figure 4B). By detecting and aligning these mEPSCs, we could average them together to resolve a deactivation time course containing two components, a fast exponential component (typically about 5 ms decay tau) and a slow exponential component (typically over 100 ms decay tau). We consider these dual-component mEPSCs to reflect the activation of AMPARs and NMDARs (Figure 4C, D, Table 5). The NMDAR antagonist APV (200 µM) eliminated the slow component of the inward current, suggesting it is entirely generated by NMDARs (Figure 4E, F). Experiments were concluded by adding the AMPAR and kainate receptor antagonist DNQX (10 µM), which blocked all mEPSCs, confirming that they reflected glutamatergic synaptic currents. Using this recording paradigm we assayed the actions of (+)-CIQ on mEPSCs from hippocampal CA1 interneurons (for observed mEPSC characteristics, Table 5; the protocol is given in Supplemental Figure S2A).

(+)-CIQ (10 µM) had no significant effect on the amplitude of the AMPAR-component of the mEPSCs (99 ± 3%, Figure 5A and C, Table 6, repeat measure ANOVA, N=17, $F(2,32) = 5.651$, $p = 0.0079$, Dunnett's test, $p < 0.05$ for APV). By contrast, (+)-CIQ enhanced the amplitude of the NMDAR-mediated

Molecular Pharmacology Fast Forward. Published on September 13, 2016 as DOI: 10.1124/mol.116.105130
This article has not been copyedited and formatted. The final version may differ from this version.

component of the mEPSC to 147 ± 10% of control (Figure 5B, D, Table 6, repeat measure ANOVA, N=17, $F(2,32) = 173.0$, $p < 0.0001$, Dunnett's test, $p < 0.05$). APV reduced the NMDAR amplitude to 18 ± 4% of control ($p < 0.001$, Dunnett's test). In vehicle experiments, the AMPAR-component amplitude of the mEPSCs did not significantly change nor did the NMDAR-component, the latter which was blocked by APV (NMDAR amplitude, 115 ± 22% vehicle/control, 14 ± 4% APV/control Figure 5E, Supplemental Figure S2B-D, Table 6, repeat measure ANOVA, N=8, $F(2,14) = 22.31$, $p < 0.0001$, Dunnett's test, $p < 0.0001$ for APV). We also recorded mEPSCs from CA1 pyramidal neurons, which should lack the GluN2D subunit (Table 5). When (+)-CIQ was applied to pyramidal neurons, there were no detectable changes in the amplitude of the AMPAR-mediated fast component of the mEPSC (94 ± 15%) or the NMDAR-mediated slow components of the mEPSCs (109 ± 19%), the latter which was sensitive to APV (10 ± 2%, Figure 5A, B, F, Supplemental Figure S2D, Table 6, repeat measure ANOVA, N=10, $F(2,18) = 76.94$, $p < 0.0001$, Dunnett's test $p>0.05$ for (+)-CIQ and $p < 0.0001$ for APV). (+)-CIQ also had no significant effect on the amplitude of the AMPAR or NMDAR component of the mEPSC in slices prepared from *GRIN2D*-/- mice (NMDAR amplitude, 90 ± 20% (+)-CIQ/control, 16 ± 3% APV/control, Figure 5A, B and G, Supplemental Figure S2D, Table 6, repeat measure ANOVA, N=4, $F(2,6) = 56.02$, $p < 0.0001$, Dunnett's test, $p > 0.05$ for (+)-CIQ and $p < 0.0001$ for APV). These data support that the potentiating effects of (+)-CIQ on interneuron mEPSCs reflect actions at the GluN2D subunit.

(+)-CIQ does not alter the NMDAR EPSC time course

We analyzed the time course of the NMDAR-component of the mean composite mEPSCs recorded in the presence of 1.5 mM extracellular Mg^{2+} at a holding current of +40 mV. These currents were larger and provide a more reliable analysis of the synaptic time course of the NMDAR-component of the mEPSC. These synaptic currents may arise from a mixed population of interneurons that have different AMPAR subtype expression. Some of these interneurons express GluA2-lacking AMPARs with inward rectifying current-voltage relationship in the presence of intracellular spermine (McBain and Dingledine 1993, Matta

Molecular Pharmacology Fast Forward. Published on September 13, 2016 as DOI: 10.1124/mol.116.105130
This article has not been copyedited and formatted. The final version may differ from this version.

2013). We measured the time course of the NMDAR component of the mEPSC in the presence of only $GABA_A$ antagonists for wild type and *GRIN2D*-/- stratum radiatum interneurons (Figure 6A). The average mEPSC response amplitude at +40 mV was 18 ± 1.2 pA in CA1 interneurons in slices from wild type mice, similar to mEPSCs in CA3 stratum radiatum interneurons (McBain and Dingledine 1993). By fitting the composite mEPSC time course to two exponential components, the amplitude of the NMDAR-component was 12 ± 1.2 pA and decayed with a tau of 200 ± 18 ms. The amplitude of the NMDAR-component under these recording conditions is likely higher than that determined at -60 mV due to the channel block produced by 0.1 mM Mg^{2+}, as well as the ability of Mg^{2+} at 1.5 mM (+40 mV) to potentiate GluN2B outward currents (Paoletti 1995). Additionally, we observed an increase in NMDAR-dependent noise in recordings at +40 mV, which altered the amplitude threshold for mEPSCs detection, potentially skewing our sample of mEPSCs to a subset with larger amplitudes. In CA1 interneurons held at +40 mV in slices from *GRIN2D*-/- mice, the mEPSC amplitude was 13 ± 1.9 pA (*GRIN2D*-/- compared to WT, unpaired t-test, p = 0.06, N=12,5). The amplitude of the NMDAR-mediated component of the *GRIN2D*-/- mEPSC was 9.7 ± 2.3 pA (*GRIN2D*-/- compared to WT, unpaired t-test, p = 0.33, N=12,5) with a tau of 300 ± 44 ms (*GRIN2D*-/- compared to WT, unpaired t-test, p = 0.02, N=12,5).

Additional experiments were performed with racemic CIQ to investigate the time course of the CIQ-responsive synaptic current (Figure 6B-D). Pairs of evoked EPSCs were recorded from hippocampal interneurons at +40 mV from P14-21 slices (Figure 6B). The evoked EPSC time course was determined in cells for which racemic CIQ produced a reversible increase of the NMDAR peak amplitude (at least 120% of control, 16 of 50 cells, Figure 6C). Potentiation of the peak amplitude in these cells was on average 142 ± 6% of control (Figure 6D). There was no detectable change by CIQ in the paired pulse ratio (Figure 6B, summary data not shown, p = 0.34, one sample t-test). In this subset of CIQ-sensitive cells, the weighted time constant was not significantly different in CIQ compared to control (Figure 6D, 110 ± 5.7% of control, n=16, p = 0.08, paired t-test).

Molecular Pharmacology Fast Forward. Published on September 13, 2016 as DOI: 10.1124/mol.116.105130
This article has not been copyedited and formatted. The final version may differ from this version.

(+)-CIQ increases spontaneous interneuron activity in mouse hippocampal brain slices.

Hippocampal CA1 interneurons exhibit tonic firing activity that can be modulated by NMDAR activity (Lacaille 1987, Xue 2011). To determine whether (+)-CIQ could influence interneuron activity through its actions on GluN2D-containing NMDARs, we recorded spontaneous inhibitory post synaptic currents (sIPSCs) from CA1 pyramidal cells from P7-14 mice. $GABA_A$ receptor-mediated sIPSCs (Figure 7A) were isolated by recording at the reversal potential of AMPARs and NMDARs (+10mV, see *Methods*). The baseline sIPSC frequency (3.51 ± 0.55 s^{-1}) was increased during application of (+)-CIQ by 1.48 ± 1.9 fold (Figure 7B, C, paired t-test, p = 0.02). In addition, (+)-CIQ significantly increase the total inhibitory charge transfer, measured as the integral of the sIPSC recordings, by 1.71 ± 0.3 fold of baseline (paired t-test t-test, p = 0.04, Figure 7C). There was no detectable difference in sIPSC peak amplitude (1.12 ± 0.12 fold of baseline, paired t-test t-test, p = 0.32).

In parallel experiments, 200 μM APV was applied to the slice, and did not detectably alter the mean sIPSC frequency (control 2.60 ± 0.54 s^{-1}, APV 2.18 ± 0.34 s^{-1}). Application of (+)-CIQ, in the presence of APV had no significant effect on sIPSC frequency (0.92 ± 0.13 fold of baseline, p = 0.56), amplitude (0.96 ± 0.08 fold of baseline, p = 0.65) or total inhibitory charge transfer (Figure 7B, C, 0.86 ± 0.15 fold of baseline, p = 0.32). These data suggest that the effects of (+)CIQ that we measured were NMDA receptor-dependent.

Molecular Pharmacology Fast Forward. Published on September 13, 2016 as DOI: 10.1124/mol.116.105130
This article has not been copyedited and formatted. The final version may differ from this version.

DISCUSSION

Three important conclusions can be drawn from this study. First, *GRIN2D* mRNA is present in a wide array of interneurons as assessed by single cell PCR and *in situ* hybridization experimentation. Second, GluN2D subunit immunoreactivity could be detected in the neuropil of all hippocampal subfields, and expression persisted in adult mice. Third, the GluN2C/GluN2D-selective positive allosteric modulator (+)-CIQ potentiates the NMDAR-component of synaptic events in WT hippocampal CA1 interneurons but not *GRIN2D*-/- interneurons. These data suggest that (+)-CIQ can increase the activity of hippocampal CA1 interneurons, which was confirmed in recordings of spontaneous IPSCs in hippocampal pyramidal cells. These data provide strong evidence that the GluN2D subunit contributes to the NMDARs that mediate excitatory synaptic transmission onto interneurons. In addition, we describe (+)-CIQ's improved pharmacological properties over its racemic mixture.

Expression of GluN2D in hippocampal interneurons has previously been inferred by various means (Monyer 1994, Thompson 2002, von Engelhardt 2015). Here, we provide direct functional pharmacological evidence supporting the expression of GluN2D at synapses in hippocampal interneurons. By contrast, GluN2D appears to be undetectable in the NMDARs that mediate excitatory synapses onto CA1 pyramidal cells at this developmental stage. Multiple lines of evidence in this study suggest that this population of synaptic NMDARs that are modulated by (+)-CIQ may be triheteromeric receptors that contain one GluN2D plus either a GluN2A or GluN2B subunit. The observed time course of the (+)-CIQ-sensitive currents (GluN2D-containing synaptic NMDAR responses) is distinct from that of recombinant diheteromeric GluN1/GluN2D NMDARs *in vitro* (Vance 2012, Wyllie 2013, Swanger 2015). Diheteromeric GluN1/GluN2D NMDARs display an unusually long decay time constant following removal of glutamate (time constant ~1 s, at 32°C). If diheteromeric GluN1/GluN2D NMDARs were present at the synapse, we would expect a slower EPSC time course than observed, regardless of the GluN1 splice variant expressed (Vance 2012) given that the deactivation rate of the receptors expressed controls the time course of the EPSC (Lester 1990). However, the absence of a detectable increase in the deactivation time course of the NMDAR

Molecular Pharmacology Fast Forward. Published on September 13, 2016 as DOI: 10.1124/mol.116.105130
This article has not been copyedited and formatted. The final version may differ from this version.

response by potentiating GluN2D-containing receptors suggests that the NMDAR pool does not contain a high portion of diheteromeric GluN1/GluN2D NMDARs. Recent data describing the time course of triheteromeric NMDARs suggest that the deactivation time course may be dominated by that of the faster deactivating subunit following rapid removal of glutamate (Hansen 2014). For example, the deactivation time course for triheteromeric GluN1/GluN2A/GluN2B NMDARs (57 ms, 23°C) was closer to that of the faster deactivating GluN1/GluN2A diheteromeric receptor (33 ms, 23°C) than the slower deactivating GluN1/GluN2B diheteromeric receptor (274 ms, 23°C, data from Hansen 2014). Thus, the EPSC time course that we detected here (200 ± 18 ms, 29-32°C) may reflect the more rapid deactivation of the GluN2 subunit that is co-assembled with GluN2D. In addition, racemic CIQ's actions on *in vitro* GluN1/GluN2A/GluN2D-containing NMDAR further suggest that (+)-CIQ acts on triheteromeric receptors in this study. The degree of potentiation by 10 μM (+)-CIQ (150%) observed here is similar to that described for CIQ actions on tri-heteromeric GluN1/GluN2A/GluN2D receptors, as opposed to diheteromeric receptors that contain 2 copies of GluN2D, which show >200% potentiation by CIQ (Mullasseril 2010). Together these data suggest GluN2D-containing diheteromeric NMDARs are either not present at the synapse or constitute a small portion of the synaptic receptor pool of NMDARs.

There is also the possibility that only a subset of synapses express synaptic GluN2D-containing NMDARs, which would reduce the experimentally measured mean effect of (+)-CIQ from all synapses (as measured by mEPSC recordings). In addition, (+)-CIQ for unanticipated reasons might not reach all synapses in the recorded slices, preventing a fully potentiated state. The evoked EPSCs recorded at positive potentials revealed that approximately 1 in 3 cells are influenced by racemic CIQ. By contrast, data obtained for mEPSCs and single cell RT-PCR experiments, in which more than 75% of the cells show evidence of *GRIN2D* expression. This discrepancy in GluN2D detection may have a systematic cause. Single-cell RT-PCR samples the complete cellular contents of the neuron and detected mEPSCs should be sampled from the entire dendritic arbor of the neuron, whereas typical stimulating protocols activate release from only 5-10 synapses (approximated from the average stimulated response amplitudes and mEPSC amplitude at +40 mV

Molecular Pharmacology Fast Forward. Published on September 13, 2016 as DOI: 10.1124/mol.116.105130
This article has not been copyedited and formatted. The final version may differ from this version.

in this study). The lower percentage of CIQ-sensitive synaptic cells may also reflect voltage-dependent plasticity of GluN2D, given the step to +40 mV might increase intracellular levels of Ca^{2+} that could momentarily overload the buffering capacity provided by the intracellular BAPTA and alter receptor expression or localization.

Our results agree with a recent study (von Engelhardt 2015), which uses genetic studies and pharmacological experiments to suggests the expression of synaptic GluN2D by analyzing the effects of a GluN2B-selective inhibitor, ifenprodil, on hippocampal CA1 interneurons in WT and *GRIN2D*-/- mice. Our data from experiments showing the actions of (+)-CIQ on mEPSCs deactivation taus suggest that the presence of a GluN2D-containing pool of synaptic NMDARs does not prolong the EPSC time course. This result differs from recent data showing that ifenprodil prolongs the EPSC time course (von Engelhardt 2015), which was interpreted to reflect the influence of GluN2D on synaptic currents in the absence of functional GluN2B. Additionally, our data with (+)-CIQ suggests that synaptic GluN2D-containing NMDARs in CA1 interneurons are potentially triheteromeric NMDARs. The discrepancy in the GluN2D-containing component of the NMDAR-EPSC synaptic time course between these two studies could be due to pharmacology of ifenprodil at these triheteromeric receptors. For instance, ifenprodil is known to increase glutamate affinity at GluN2B-containing NMDARs (Kew and Kemp 1998), which slows the deactivation time course, an effect that might be pronounced in GluN2B/GluN2D triheteromeric NMDARs. A complete study of ifenprodil's actions at all possible triheteromeric receptors that can be made with GluN2A, GluN2B and GluN2D will need to be assessed to fully interpret these observations.

Interestingly, we detected a slower NMDAR synaptic time course in *GRIN2D*-/- neurons (300 ± 44 ms) than WT neurons (200 ± 18 ms), consistent with the result reported by von Engelhardt (2015) who showed at a lower recording temperature and different animal age a prolongation of the median time constant from 253 ms in WT mice to and 323 ms in *GRIN2D*-/- mice. This result is paradoxical since GluN2D has a longer deactivation time course, and the loss of GluN2D would therefore be expected to shorten the net NMDA deactivation time course, as is observed in the spinal cord and subthalamic nuclei (Hildebrand 2014,

Molecular Pharmacology Fast Forward. Published on September 13, 2016 as DOI: 10.1124/mol.116.105130
This article has not been copyedited and formatted. The final version may differ from this version.

Swanger 2015). This may reflect an overall difference in GluN2D expression or differences in GluN2D-containing NMDAR composition. Additionally, the *GRIN2D*-/- mice might have a disrupted GluN2A/GluN2B developmental switch that gives rise to this observed deactivation time course at this age (Liu 2004, Lu and Constantine-Paton 2004), or other compensatory mechanisms that alter the properties of synaptic receptors. More work needs to be done to further understand how specific NMDAR subunits such as GluN2D influence circuit-, network-, and systems-level dynamics

The finding that GluN2D is expressed in hippocampal interneurons has important implications for circuit function, exemplified by the ability of (+)-CIQ to increase the activity of CA1 interneurons. The presence of GluN2D could enable a different role of NMDARs in these cell types and in the hippocampal network. Co-assembly of GluN2D may change open probability and trafficking of synaptic receptors, and consequently alter where these receptors are expressed, what signals (i.e. synaptic, peri-synaptic, extra-synaptic) they receive, and how these signals are integrated. The interneurons of the hippocampus as well as neocortex control the excitability of local circuits, influencing other interneurons as well as principle cells, and thus sculpting the firing patterns of pyramidal/projection neurons. Furthermore, the GluN2D subunit may dictate distinct rules for the firing patterns that are capable of triggering NMDAR-dependent synaptic plasticity. If potentiation of GluN2D changes the synaptic NMDAR response to be more GluN2D-like (low open probability, low Ca^{2+} permeability, weak Mg^{2+} block) when the population of receptors are mixed, neuronal plasticity that depends on these properties, such as spike timing-dependent plasticity, may be altered by GluN2D potentiation (Hao and Oertner 2012, Verhoog 2013, Stefanescu and Shore 2015). A complete understanding of the pharmacology of triheteromeric NMDARs containing GluN2D is required to understand how these receptors are behaving in the hippocampus. As shown by the increase in sIPSC frequency by (+)-CIQ, positive allosteric modulation of GluN2D-containing NMDARs could have important effects on circuit and network function. The ability of GluN2C/D-selective modulators to alter the network balance of hippocampus by selectively acting on interneurons (Bachtiar and Stagg 2014, Talaei 2016) might have significant actions on animal behavior, such as learning and memory (Kullmann and Lamsa 2007,

Molecular Pharmacology Fast Forward. Published on September 13, 2016 as DOI: 10.1124/mol.116.105130
This article has not been copyedited and formatted. The final version may differ from this version.

Sweatt 2016). In addition, modulation of interneuron activity by GluN2C/D-selective allosteric modulators could have therapeutic implications (Collingridge 2013).

Molecular Pharmacology Fast Forward. Published on September 13, 2016 as DOI: 10.1124/mol.116.105130
This article has not been copyedited and formatted. The final version may differ from this version.

ACKNOWLEDGEMENTS

We thank Phoung Le and Jing Zhang for outstanding technical assistance. We also thank Susan Jenkins and Jean-Francois Pare for help with immunostaining. K_i determinations and receptor binding profiles were generously provided by the National Institute of Mental Health's Psychoactive Drug Screening Program, Contract # HHSN-271-2013-00017-C (NIMH PDSP). The NIMH PDSP is directed by Bryan L. Roth MD, PhD at the University of North Carolina at Chapel Hill and Project Officer Jamie Driscoll at NIMH, Bethesda MD, USA.

Molecular Pharmacology Fast Forward. Published on September 13, 2016 as DOI: 10.1124/mol.116.105130
This article has not been copyedited and formatted. The final version may differ from this version.

AUTHORSHIP CONTRIBUTIONS

Participated in research design: Perszyk, DiRaddo, Strong, Low, Ogden, Khatri, Vargish, Pelkey, Tricoire, Liotta, Smith, McBain, and Traynelis.

Conducted experiments: Perszyk, DiRaddo, Low, Ogden, Khatri, Vargish, Pelkey, Tricoire, Smith.

Contributed new reagents or analytic tools: Strong, Liotta.

Performed data analysis: Perszyk, DiRaddo, Low, Ogden, Khatri, Vargish, Pelkey, Tricoire, Smith.

Wrote or contributed to the writing of the manuscript: Perszyk, DiRaddo, Strong, Low, Ogden, Khatri, Vargish, Pelkey, Tricoire, Liotta, Smith, McBain, and Traynelis.

Molecular Pharmacology Fast Forward. Published on September 13, 2016 as DOI: 10.1124/mol.116.105130
This article has not been copyedited and formatted. The final version may differ from this version.

REFERENCES

Akazawa, C., R. Shigemoto, Y. Bessho, S. Nakanishi and N. Mizuno (1994). Differential expression of five N-methyl-D-aspartate receptor subunit mRNAs in the cerebellum of developing and adult rats. *The Journal of Comparative Neurology* **347**(1): 150-160.

Bachtiar, V. and C. J. Stagg (2014). The role of inhibition in human motor cortical plasticity. *Neuroscience* **278**: 93-104.

Besnard, J., G. F. Ruda, V. Setola, K. Abecassis, R. M. Rodriguiz, X.-P. Huang, S. Norval, M. F. Sassano, A. I. Shin, L. A. Webster, F. R. C. Simeons, L. Stojanovski, A. Prat, N. G. Seidah, D. B. Constam, G. R. Bickerton, K. D. Read, W. C. Wetsel, I. H. Gilbert, B. L. Roth and A. L. Hopkins (2012). Automated design of ligands to polypharmacological profiles. *Nature* **492**(7428): 215-220.

Cauli, B., E. Audinat, B. Lambolez, M. C. Angulo, N. Ropert, K. Tsuzuki, S. Hestrin and J. Rossier (1997). Molecular and Physiological Diversity of Cortical Nonpyramidal Cells. *The Journal of Neuroscience* **17**(10): 3894-3906.

Cauli, B., J. T. Porter, K. Tsuzuki, B. Lambolez, J. Rossier, B. Quenet and E. Audinat (2000). Classification of fusiform neocortical interneurons based on unsupervised clustering. *Proc Natl Acad Sci U S A* **97**(11): 6144-6149.

Choi, D. W. (1992). Excitotoxic cell death. *Journal of Neurobiology* **23**(9): 1261-1276.

Clarke, R. J. and J. W. Johnson (2006). NMDA Receptor NR2 Subunit Dependence of the Slow Component of Magnesium Unblock. *The Journal of Neuroscience* **26**(21): 5825-5834.

Collingridge, G. L., A. Volianskis, N. Bannister, G. France, L. Hanna, M. Mercier, P. Tidball, G. Fang, M. W. Irvine, B. M. Costa, D. T. Monaghan, Z. A. Bortolotto, E. Molnar, D. Lodge and D. E. Jane (2013). The NMDA receptor as a target for cognitive enhancement. *Neuropharmacology* **64**: 13-26.

Coyle, J. T. (2012). NMDA Receptor and Schizophrenia: A Brief History. *Schizophrenia Bulletin* **38**(5): 920-926.

Coyle, J. T., G. Tsai and D. Goff (2003). Converging evidence of NMDA receptor hypofunction in the pathophysiology of schizophrenia. *Ann N Y Acad Sci* **1003**: 318-327.

Edman, S., S. McKay, L. J. MacDonald, M. Samadi, M. R. Livesey, G. E. Hardingham and D. J. A. Wyllie (2012). TCN 201 selectively blocks GluN2A-containing NMDARs in a GluN1 co-agonist dependent but non-competitive manner. *Neuropharmacology* **63**(3): 441-449.

Hallett, P. J. and D. G. Standaert (2004). Rationale for and use of NMDA receptor antagonists in Parkinson's disease. *Pharmacol Ther* **102**(2): 155-174.

Hansen, Kasper B., Kevin K. Ogden, H. Yuan and Stephen F. Traynelis (2014). Distinct Functional and Pharmacological Properties of Triheteromeric GluN1/GluN2A/GluN2B NMDA Receptors. *Neuron* **81**(5): 1084-1096.

Hansen, K. B., N. Tajima, R. Risgaard, R. E. Perszyk, L. Jorgensen, K. M. Vance, K. K. Ogden, R. P. Clausen, H. Furukawa and S. F. Traynelis (2013). Structural Determinants of Agonist Efficacy at the Glutamate Binding Site of NMDA Receptors. *Molecular Pharmacology*.

Hao, J. and T. G. Oertner (2012). Depolarization gates spine calcium transients and spike-timing-dependent potentiation. *Current Opinion in Neurobiology* **22**(3): 509-515.

Hildebrand, M. E., G. M. Pitcher, E. K. Harding, H. Li, S. Beggs and M. W. Salter (2014). GluN2B and GluN2D NMDARs dominate synaptic responses in the adult spinal cord. *Scientific Reports* **4**: 4094.

Kew, J. N. C. and J. A. Kemp (1998). An allosteric interaction between the NMDA receptor polyamine and ifenprodil sites in rat cultured cortical neurones. *The Journal of Physiology* **512**(1): 17-28.

Kullmann, D. M. and K. P. Lamsa (2007). Long-term synaptic plasticity in hippocampal interneurons. *Nat Rev Neurosci* **8**(9): 687-699.

Lacaille, J. C., A. L. Mueller, D. D. Kunkel and P. A. Schwartzkroin (1987). Local circuit interactions between oriens/alveus interneurons and CA1 pyramidal cells in hippocampal slices: electrophysiology and morphology. *J Neurosci* **7**(7): 1979-1993.

Lambolez, B., E. Audinat, P. Bochet, F. Crépel and J. Rossier (1992). AMPA receptor subunits expressed by single purkinje cells. *Neuron* **9**(2): 247-258.

Landwehrmeyer, G., D. Standaert, C. Testa, J. Penney and A. Young (1995). NMDA receptor subunit mRNA expression by projection neurons and interneurons in rat striatum. *The Journal of Neuroscience* **15**(7): 5297-5307.

Lester, R. A. J., J. D. Clements, G. L. Westbrook and C. E. Jahr (1990). Channel kinetics determine the time course of NMDA receptor-mediated synaptic currents. *Nature* **346**(6284): 565-567.

Liu, X.-B., K. D. Murray and E. G. Jones (2004). Switching of NMDA Receptor 2A and 2B Subunits at Thalamic and Cortical Synapses during Early Postnatal Development. *The Journal of Neuroscience* **24**(40): 8885-8895.

Lu, W. and M. Constantine-Paton (2004). Eye Opening Rapidly Induces Synaptic Potentiation and Refinement. *Neuron* **43**(2): 237-249.

Matta, J. A., K. A. Pelkey, M. T. Craig, R. Chittajallu, B. W. Jeffries and C. J. McBain (2013). Developmental origin dictates interneuron AMPA and NMDA receptor subunit composition and plasticity. *Nat Neurosci* **16**(8): 1032-1041.

McBain, C. J. and R. Dingledine (1993). Heterogeneity of synaptic glutamate receptors on CA3 stratum radiatum interneurones of rat hippocampus. *The Journal of Physiology* **462**(1): 373-392.

McKay, S., N. H. Griffiths, P. A. Butters, E. B. Thubron, G. E. Hardingham and D. J. A. Wyllie (2012). Direct pharmacological monitoring of the developmental switch in NMDA receptor subunit composition using TCN 213, a GluN2A-selective, glycine-dependent antagonist. *British Journal of Pharmacology* **166**(3): 924-937.

Monyer, H., N. Burnashev, D. J. Laurie, B. Sakmann and P. H. Seeburg (1994). Developmental and regional expression in the rat brain and functional properties of four NMDA receptors. *Neuron* **12**(3): 529-540.

Mullasseril, P., K. B. Hansen, K. M. Vance, K. K. Ogden, H. Yuan, N. L. Kurtkaya, R. Santangelo, A. G. Orr, P. Le, K. M. Vellano, D. C. Liotta and S. F. Traynelis (2010). A subunit-selective potentiator of NR2C- and NR2D-containing NMDA receptors. *Nat Commun* **1**: 90.

Palmer, G. C. (2001). Neuroprotection by NMDA Receptor Antagonists in a Variety of Neuropathologies. *Current Drug Targets* **2**(3): 241-271.

Paoletti, P., J. Neyton and P. Ascher (1995). Glycine-independent and subunit-specific potentiation of NMDA responses by extracellular Mg2+. *Neuron* **15**(5): 1109-1120.

Pelkey, Kenneth A., E. Barksdale, Michael T. Craig, X. Yuan, M. Sukumaran, Geoffrey A. Vargish, Robert M. Mitchell, Megan S. Wyeth, Ronald S. Petralia, R. Chittajallu, R.-M. Karlsson, Heather A. Cameron, Y. Murata, Matthew T. Colonnese, Paul F. Worley and Chris J. McBain (2015). Pentraxins Coordinate Excitatory Synapse Maturation and Circuit Integration of Parvalbumin Interneurons. *Neuron* **85**(6): 1257-1272.

Pelkey, K. A., G. Lavezzari, C. Racca, K. W. Roche and C. J. McBain (2005). mGluR7 is a metaplastic switch controlling bidirectional plasticity of feedforward inhibition. *Neuron* **46**(1): 89-102.

Pelkey, K. A., L. Topolnik, J. C. Lacaille and C. J. McBain (2006). Compartmentalized Ca(2+) channel regulation at divergent mossy-fiber release sites underlies target cell-dependent plasticity. *Neuron* **52**(3): 497-510.

Porter, J. T., B. Cauli, J. F. Staiger, B. Lambolez, J. Rossier and E. Audinat (1998). Properties of bipolar VIPergic interneurons and their excitation by pyramidal neurons in the rat neocortex. *Eur J Neurosci* **10**(12): 3617-3628.

Preskorn, S., M. Macaluso, D. V. Mehra, G. Zammit, J. R. Moskal, R. M. Burch and t. G.-C. S. Group (2015). Randomized Proof of Concept Trial of GLYX-13, an N-Methyl-D-Aspartate Receptor Glycine Site Partial Agonist, in Major Depressive Disorder Nonresponsive to a Previous Antidepressant Agent. *Journal of Psychiatric Practice®* **21**(2): 140-149.

Preskorn, S. H., B. Baker, S. Kolluri, F. S. Menniti, M. Krams and J. W. Landen (2008). An Innovative Design to Establish Proof of Concept of the Antidepressant Effects of the NR2B Subunit Selective N-Methyl-D-Aspartate Antagonist, CP-101,606, in Patients With Treatment-Refractory Major Depressive Disorder. *Journal of Clinical Psychopharmacology* **28**(6): 631-637.

Retchless, B. S., W. Gao and J. W. Johnson (2012). A single GluN2 subunit residue controls NMDA receptor channel properties via intersubunit interaction. *Nat Neurosci* **15**(3): 406-413.

Rudolf, G. D., C. A. Cronin, G. B. Landwehrmeyer, D. G. Standaert, J. B. Penney, Jr. and A. B. Young (1996). Expression of N-methyl-D-aspartate glutamate receptor subunits in the prefrontal cortex of the rat. *Neuroscience* **73**(2): 417-427.

Santangelo Freel, R., K. Ogden, K. Strong, A. Khatri, K. Chepiga, H. Jensen, S. Traynelis and D. Liotta (2013). Synthesis and structure activity relationship of tetrahydroisoquinoline-based potentiators of GluN2C and GluN2D containing N-methyl-D-aspartate receptors. *Journal of medicinal chemistry* **56**(13): 5351-5381.

Santangelo Freel, R. M., K. K. Ogden, K. L. Strong, A. Khatri, K. M. Chepiga, H. S. Jensen, S. F. Traynelis and D. C. Liotta (2014). Correction to Synthesis and Structure Activity Relationship of Tetrahydroisoquinoline-Based Potentiators of GluN2C and GluN2D Containing N-Methyl-d-aspartate Receptors. *Journal of Medicinal Chemistry* **57**(11): 4975-4975.

Standaert, D. G., G. Bernhard Landwehrmeyer, J. A. Kerner, J. B. Penney Jr and A. B. Young (1996). Expression of NMDAR2D glutamate receptor subunit mRNA in neurochemically identified interneurons in the rat neostriatum, neocortex and hippocampus. *Molecular Brain Research* **42**(1): 89-102.

Standaert, D. G., C. M. Testa, A. B. Young and J. B. Penney (1994). Organization of N-methyl-D-aspartate glutamate receptor gene expression in the basal ganglia of the rat. *The Journal of Comparative Neurology* **343**(1): 1-16.

Stefanescu, R. A. and S. Shore (2015). NMDA receptors mediate stimulus-timing-dependent plasticity and neural synchrony in the dorsal cochlear nucleus. *Frontiers in Neural Circuits* **9**.

Swanger, S. A., K. M. Vance, J.-F. Pare, F. Sotty, K. Fog, Y. Smith and S. F. Traynelis (2015). NMDA Receptors Containing the GluN2D Subunit Control Neuronal Function in the Subthalamic Nucleus. *The Journal of Neuroscience* **35**(48): 15971-15983.

Sweatt, J. D. (2016). Neural plasticity and behavior – sixty years of conceptual advances. *Journal of Neurochemistry*.

Talaei, S. A., A. Azami and M. Salami (2016). Postnatal development and sensory experience synergistically underlie the excitatory/inhibitory features of hippocampal neural circuits: Glutamatergic and GABAergic neurotransmission. *Neuroscience* **318**: 230-243.

Thompson, C. L., D. L. Drewery, H. D. Atkins, F. A. Stephenson and P. L. Chazot (2002). Immunohistochemical localization of N-methyl-d-aspartate receptor subunits in the adult murine hippocampal formation: evidence for a unique role of the NR2D subunit. *Molecular Brain Research* **102**(1-2): 55-61.

Traynelis, S. F., L. P. Wollmuth, C. J. McBain, F. S. Menniti, K. M. Vance, K. K. Ogden, K. B. Hansen, H. Yuan, S. J. Myers and R. Dingledine (2010). Glutamate Receptor Ion Channels: Structure, Regulation, and Function. *Pharmacological Reviews* **62**(3): 405-496.

Vance, K. M., K. B. Hansen and S. F. Traynelis (2012). GluN1 splice variant control of GluN1/GluN2D NMDA receptors. *The Journal of Physiology* **590**(16): 3857-3875.

Vance, K. M., K. B. Hansen and S. F. Traynelis (2013). Modal gating of GluN1/GluN2D NMDA receptors. *Neuropharmacology* **71**: 184-190.

Verhoog, M. B., N. A. Goriounova, J. Obermayer, J. Stroeder, J. J. J. Hjorth, G. Testa-Silva, J. C. Baayen, C. P. J. de Kock, R. M. Meredith and H. D. Mansvelder (2013). Mechanisms Underlying the Rules for Associative Plasticity at Adult Human Neocortical Synapses. *The Journal of Neuroscience* **33**(43): 17197-17208.

Vicini, S., J. F. Wang, J. H. Li, W. J. Zhu, Y. H. Wang, J. H. Luo, B. B. Wolfe and D. R. Grayson (1998). Functional and Pharmacological Differences Between RecombinantN-Methyl-d-Aspartate Receptors. *Journal of Neurophysiology* **79**(2): 555-566.

von Engelhardt, J., C. Bocklisch, L. Tönges, A. Herb, M. Mishina and H. Monyer (2015). GluN2D-containing NMDA receptors-mediate synaptic currents in hippocampal interneurons and pyramidal cells in juvenile mice. *Frontiers in Cellular Neuroscience* **9**.

Wyllie, D. J. A., M. R. Livesey and G. E. Hardingham (2013). Influence of GluN2 subunit identity on NMDA receptor function. *Neuropharmacology* **74**: 4-17.

Xue, J.-G., T. Masuoka, X.-D. Gong, K.-S. Chen, Y. Yanagawa, S. K. A. Law and S. Konishi (2011). NMDA receptor activation enhances inhibitory GABAergic transmission onto hippocampal pyramidal neurons via presynaptic and postsynaptic mechanisms. *Journal of Neurophysiology* **105**(6): 2897-2906.

Yuan, H., C.-M. Low, O. A. Moody, A. Jenkins and S. F. Traynelis (2015). Ionotropic GABA and Glutamate Receptor Mutations and Human Neurologic Diseases. *Molecular Pharmacology* **88**(1): 203-217.

Footnotes

This work was supported by the National Institutes of Health National Institute of Neurological Disorders and Stroke [Grants RO1-NS036654, RO1-NS065371]; National Institutes of Health National Institute of General Medical Sciences [Grant T32-GM008602]; and National Institutes of Health Office of Research Infrastructure Programs [Grant P51OD011132]. This research was supported [in part] by the Intramural Research Program of the National Institutes of Health [National Institute of Child Health and Human Development].

Dennis Liotta, Katie Strong and Stephen Traynelis are inventors on Emory-owned IP. Dennis Liotta is a member of the Board of Directors and Stephen Traynelis is a paid consultant for NeurOp Inc., a company developing NMDA receptor modulators. Stephen Traynelis is a paid consultant for Pfizer and Janssen Research and Development. We thank Sharon Swanger for critical comments on the manuscript.

Molecular Pharmacology Fast Forward. Published on September 13, 2016 as DOI: 10.1124/mol.116.105130
This article has not been copyedited and formatted. The final version may differ from this version.

FIGURE LEGENDS

Figure 1. (+)-CIQ but not (–)-CIQ potentiates NMDA receptor-mediated currents in *X. laevis* oocytes. (**A)** Representative response of a GluN1/GluN2D NMDAR (activated by 100 μM glutamate and 30 μM glycine) in the absence and presence of increasing concentrations of (+)-CIQ (0, 0.3, 1, 3, 10, 30 μM). (**B)** The chemical structure of CIQ is shown with the chiral carbon indicated by the asterisk (Santangelo Freel 2013, Santangelo Freel 2014). (**C-F)** Concentration-response relationships show the effects of the purified enantiomers of (+)-CIQ, (-)-CIQ and racemic CIQ on the diheteromeric NMDARs, recorded under two electrode voltage clamp from *X. laevis* oocytes. (**G)** Off-target effects of 20 μM (+)- and (-)-CIQ on a subset of CNS receptors expressed in *X. laevis* oocytes (see *Methods*).

Figure 2. Characterization of *GRIN2D* mRNA expression in sub-types of CA1 hippocampal interneurons. (**A)** Flattened 2D maximum projection image of a representative interneuron recorded in stratum oriens. (**B**) Example membrane potential response recorded under current clamp to the square wave current injection (±400 pA) protocol indicated below (scale bars 500 ms / 20 mV). (**C**) Single cell RT-PCR products from the neuron shown in (**A**) reveal expression of PV, SOM, NPY, GAD65/67, *GRIN1*, *GRIN2A*, *GRIN2B* and *GRIN2D* (*Upper panel*). The lower panel shows RT-PCR products from 100 ng whole brain total RNA, confirming that all primer pairs generate appropriate bands. (**D, E, F**) Representative fluorescence *in situ* hybridization images from P25 mice depicting the colocalization of the *GRIN2D* and interneuron markers (**D** parvalbumin, **E** CB1R is a marker of CCK interneurons, **F** somatostatin)

Figure 3. GluN2D protein expression across development and hippocampus subfield. (**A**) Images of mouse brain slices illustrating typical tissue punches (diameter 0.75 mm) taken for protein analysis of (from left to right) the dentate gyrus, CA1, CA3, and a dissected whole hippocampus slice. (**B**) Representative western blot for GluN2D and tubulin from three different animals (p74) for the CA1, CA3 and dentate gyrus tissue punch samples. (**C**) Representative western blot of GluN2D and tubulin from whole hippocampus

slices from wild type mice aged P9, P17, P30, P58 and *GRIN2D*-/- aged P9. (**D**) Densitometry measurements for the GluN2D levels normalized to tubulin, analyzed by one-way repeat measure ANOVA (N=3, $F(2,4)$ = 8.869, p = 0.034, Tukey's multiple comparison test, comparisons that were $p < 0.05$ are denoted by *). Measurements from six replicate SDS-PAGE gels and western blots were used to produce the average for each animal's value. (**E**) Densitometry measurements for the GluN2D levels as a function of age of wild type samples normalized to tubulin, analyzed by one-way ANOVA (N=3, $F(3,8)$ = 3.95, p = 0.054). Measurements from three replicate SDS-PAGE gels and western blots were used to produce the average for each animal's protein value.

Figure 4. Characterization of mEPSCs in hippocampal CA1 interneurons from P7-14 mice. (**A**) Visible light image of a mouse hippocampal slice showing a CA1 stratum radiatum interneuron in the whole-cell patch-clamp configuration; the outline of the recording electrode has been enhanced. (**B**) An illustrative recording (filtered at 0.25 kHz) of spontaneous glutamatergic activity from a CA1 interneuron in the presence of 0.5 µM TTX, 10 µM bicuculline, and 5 µM nimodipine. (**C**) Superimposed mEPSCs (black) and the mean response time course (white); the red dashed line illustrates pre-mEPSC baseline current level. (**D**) The mEPSC peak response amplitude histogram from the interneuron recording is shown in (**C**), the patterned area indicates amplitudes below the detection threshold. (**E**) Averaged composite mEPSC time course is shown for control conditions and in APV (200 µM); the difference current reveals the NMDAR-component of the mEPSC (average response is shown ± SEM indicated by the shaded area). (**F**) The same recordings in (**E**) but at an expanded scale to better illustrate the NMDAR-component.

Figure 5. (+)-CIQ potentiates NMDAR currents in hippocampal CA1 stratum radiatum interneurons but not CA1 pyramidal neuron or in *GRIN2D*-/- interneurons from P7-14 mice. (**A**) The average composite mEPSC response from each phase of the mEPSC experiment is shown. (**B**) Composite-APV difference current reveals the NMDAR-component of the mEPSC waveform. (**C**) The AMPAR amplitudes

Molecular Pharmacology Fast Forward. Published on September 13, 2016 as DOI: 10.1124/mol.116.105130
This article has not been copyedited and formatted. The final version may differ from this version.

are shown for WT interneurons before and during (+)-CIQ application. (**D**) The measured mean NMDAR responses are shown for WT interneurons before and during (+)-CIQ application. (**E**) The measured mean NMDAR responses from WT interneurons before and during application of vehicle. (**F**) The measured mean NMDAR responses are shown from WT pyramidal cell (+)-CIQ recordings. (**G**) The measured mean NMDAR responses are shown from *GRIN2D*-/- interneurons before and during (+)-CIQ application. * indicates $p<0.05$ by Dunnett's test. 10 μM (+)-CIQ, 200 μM APV.

Figure 6. Synaptic response time course for GluN2D-containing receptors. (**A**) Normalized mEPSCs (V_{Hold} +40 mV) from wild type and *GRIN2D*-/- interneurons (P7-14) are superimposed (20% scale bar corresponds to 3.2 pA for wild type and 2.6 pA for *GRIN2D*-/-). (**B**) Time course plot of EPSC-NMDA amplitude for a representative interneuron that displayed reversible potentiation by racemic CIQ. Each point represents the peak amplitude of an individual EPSC-NMDA (first peak in paired pulse experiments, shown above) evoked at 0.2 Hz before, during, and after CIQ (10 μM) treatment. At the end of an experiment, slices were treated with the NMDAR antagonist APV (100 μM) to confirm that current responses were mediated by NMDAR activation. Current responses above are superimposed pairs of evoked average EPSC waveforms (30 consecutive events) obtained at the times indicated (scale bars 200 ms / 100 pA); expanded traces (right) show the first peak. (**C**) Fold change in the peak amplitude of responding cells (right, magenta shaded) and non-responding cells (left, blue and unshaded) during CIQ application, on brain slices from mice P14-21, and during the wash out period are shown in the left graph. Box and whiskers plots illustrate the 2.5-97.5 percentile range of the data. Responders are defined as a showing a reversible increase in current amplitude of 20% or more. In the right graph, the weighted time constant of the responding cells is shown during the CIQ and wash out periods as fold-change from pre-treatment control. Data are expressed as percentage of control EPSCs obtained prior to racemic CIQ treatment.

Molecular Pharmacology Fast Forward. Published on September 13, 2016 as DOI: 10.1124/mol.116.105130
This article has not been copyedited and formatted. The final version may differ from this version.

Figure 7. (+)-CIQ increases spontaneous interneuron activity in hippocampal brain slices from P7-14 mice. (**A**) Representative sIPSC recordings from CA1 pyramidal cells before and during the application of (+)-CIQ. (**B**) Composite rolling average (30s window of sIPSC frequency from CA1 pyramidal cells in the presence of (+)-CIQ and (+)-CIQ/APV. A baseline sIPSC frequency was established (white box, aCSF/DMSO for (+)-CIQ recordings and aCSF/200 μM APV/DMSO for (+)-CIQ/APV recordings) followed by the addition of 10 μM (+)-CIQ (grey box). Experiments ended in 10 μM gabazine (black box) to ensure spontaneous sIPSCs reflected solely $GABA_A$ receptor-mediated transmission. The shaded area shows SEM across cells. (**C**) Average change (fold over baseline response) in sIPSC frequency, amplitude and integral of current response of spontaneous activity for (+)-CIQ and (+)-CIQ/APV recordings. * indicates $p < 0.05$ by unpaired t-test of fold change over baseline for test conditions.

Molecular Pharmacology Fast Forward. Published on September 13, 2016 as DOI: 10.1124/mol.116.105130
This article has not been copyedited and formatted. The final version may differ from this version.

TABLES

Table 1. Semi-preparatory chiral column conditions and retention times of each enantiomer

	ChiralPak OD-RH solvent composition				ChiralPak OD-RH retention time	
	ACN	**H_2O**	**Flow rate (mL/min)**	**Run time (min)**	**Peak 1 (min)**	**Peak 2 (min)**
CIQ	75%	25%	10	40	24.04	27.68
BIQ	75%	25%	10	30	25.62	27.56
IIQ	65%	35%	10	40	30.06	35.27
FIQ	60%	40%	10	40	24.28	27.36

Molecular Pharmacology Fast Forward. Published on September 13, 2016 as DOI: 10.1124/mol.116.105130
This article has not been copyedited and formatted. The final version may differ from this version.

Table 2. Analytical chiral column conditions and characterization of each enantiomer

	Analytical OD-RH solvent composition				ChiralPak OD-RH retention time		Optical rotation values	
	ACN	H_2O	Flow rate (mL/min)	Run time (min)	Peak 1 (min)	Peak 2 (min)	Peak 1 (degrees)	Peak 2 (degrees)
CIQ	75%	25%	0.5	20	16.81	19.32	+121 (c 0.10, dry DMSO)	-145 (c 0.10, dry DMSO)
BIQ	75%	25%	0.5	20	8.61	9.79	+104 (c 0.1, dry $CHCl_3$)	-128 (c 0.1, dry $CHCl_3$)
IIQ	65%	35%	0.5	30	17.33	19.89	+106 (c 0.1, dry $CHCl_3$)	-93 (c 0.1, dry $CHCl_3$)
FIQ	60%	40%	0.5	30	13.47	15.53	+89.4 (c 1.0, dry $CHCl_3$)	-102 (c 1.0, dry $CHCl_3$)

Molecular Pharmacology Fast Forward. Published on September 13, 2016 as DOI: 10.1124/mol.116.105130
This article has not been copyedited and formatted. The final version may differ from this version.

Table 3: Stereoselective potentiation of GluN2C- and GluN2D-containing NMDARs

	I (30 μM) / I (control) (%)				EC_{50} (μM) [conf. int.][a] (% max. modulation)	
Compound	**GluN2A**	**GluN2B**	**GluN2C**	**GluN2D**	**GluN2C**	**GluN2D**
(+)-FIQ	100 ± 2.9	102 ± 2.1	192 ± 6.4	177 ± 3.5	N.A.	N.A.
(-)-FIQ	97 ± 0.9	96 ± 0.9	102 ± 3.5	106 ± 4.9	N.E.	N.E.
(+)-CIQ	118 ± 1.9	98 ± 1.3	250 ± 15	285 ± 11	7.8 [6.8, 9.0] (286 ± 23)	10.5 [9.5, 11.7] (322 ± 18)
(-)-CIQ	105 ± 2.7	88 ± 2.7	125 ± 4.7	117 ± 5.6	N.E.	N.E.
(+)-BIQ	87 ± 0.5	99 ± 0.8	318 ± 28	326 ± 16	3.8 [3.2, 4.5] (352 ± 47)	5.5 [5.1, 6.0] (354 ± 21)
(-)-BIQ	89 ± 5.7	84 ± 0.6	100 ± 5.0	96 ± 3.2	N.E.	N.E.
(+)-IIQ	98 ± 1.4	97 ± 0.7	197 ± 14	273 ± 15	2.1 [1.9, 2.2] (204 ± 16)	3.5 [3.1, 4.0] (289 ± 16)
(-)-IIQ	88 ± 3.6	85 ± 1.3	98 ± 5.4	85 ± 3.8	N.E.	N.E.

Values for current ratio and EC_{50} are mean ± SEM from 8-22 oocytes obtained from at least 2 different frogs.

[a] is the mean half-maximally effective concentration of modulators (see Methods). The value [95%confidence interval] was determined from fitting individual concentration-effect curves and averaging the fitted values on the *log* scale, and presented on linear scale. The Hill slopes ranged between 0.5-1.5. The fitted maximal response as a percent of control is given in parentheses.

N.A. – Not analyzed; the concentration-effect curve could not be fitted by the Hill equation

N.E. – No effect; the ratio of current in 30 μM test compound to control current was less than 130%, our threshold for further analysis.

Molecular Pharmacology Fast Forward. Published on September 13, 2016 as DOI: 10.1124/mol.116.105130
This article has not been copyedited and formatted. The final version may differ from this version.

Table 4: Single cell RT-PCR results from 37 neurons from mice P14-21

	GRIN1	*GRIN2A*	*GRIN2B*	*GRIN2C*	*GRIN2D*
Interneuron Marker	Percent of cells expressing marker				
PV expressing	100%	78%	78%	11%	67%
SOM expressing	95%	81%	86%	0%	81%
NPY expressing	86%	75%	86%	4%	79%
CCK expressing	100%	57%	86%	0%	100%
Firing Properties					
Fast Spiking	100%	50%	75%	25%	50%
Regular Spiking	88%	73%	85%	0%	82%
Soma Location					
slm	80%	80%	60%	0%	60%
so	94%	81%	88%	6%	81%
sr	87%	60%	93%	0%	87%
All Interneurons					
Detection Count	33	26	31	1	29
Percentage	89%	70%	84%	3%	78%

After harvesting the intracellular contents of each recorded cell, soma localization was evaluated using fluorescence microscopy and assigned to stratum oriens (so), stratum pyramidale (sp), stratum radiatum (sr), stratum lacunosum moleculare (slm), stratum granulosum (sg) and or hilus. Cells were categorized as fast spiking (FS) if they sustained high frequency (>150 Hz) action potential discharge with little or no decrement in spike amplitude during a strong depolarizing current pulse of long duration (1 nA, 800-1000ms), or regular spiking (RS) if they exhibited significant accommodation in spike frequency and decreasing spike amplitude during the same depolarizing current injection. See Supplemental Table S2 for explicit results from all cells.

Molecular Pharmacology Fast Forward. Published on September 13, 2016 as DOI: 10.1124/mol.116.105130
This article has not been copyedited and formatted. The final version may differ from this version.

Table 5. Measured mEPSC characteristics of neurons from P7-14 mice

	AMPAR Time Constant (ms)	NMDAR Time Constant (ms)	AMPAR Amplitude (pA)	NMDAR Amplitude (pA)[a]	mEPSC Detection rate (s^{-1})	AMPAR/ NMDAR ratio[b]	N
Interneuron Wild Type	4.6 ± 0.5	138 ± 37	20 ± 1.6	2.1 ± 0.2	1.6 ± 0.4	9.7 ± 1.1	25
Interneuron *GRIN2D*-/-	3.9 ± 0.7	140 ± 48	24 ± 4.3	3.9 ± 1.3	1.0 ± 0.5	6.8 ± 0.7	4
Pyramidal Wild Type	6.5 ± 0.4	91 ± 8.6	21 ± 1.4	4.7 ± 0.6	0.92 ± 0.22	5.9 ± 0.9	17

[a] NMDAR amplitude is calculated from the amplitude of slower component of the dual exponential fit. [b] Recordings were performed in 0.1 mM Mg^{2+}. Values are mean ± SEM; N is the number of cells recorded from.

Molecular Pharmacology Fast Forward. Published on September 13, 2016 as DOI: 10.1124/mol.116.105130
This article has not been copyedited and formatted. The final version may differ from this version.

Table 6: Effects of (+)-CIQ on the AMPAR and NMDAR components of mEPSCs in P7-14 mice

	AMPAR Amplitude[a]			NMDAR Amplitude[b]			N
	Control (pA)	Treatment (pA)	Treatment/ Control	Control (pA)	Treatment (pA)	Treatment/ Control	
Interneuron							
Wild Type Vehicle	18 ± 3.4	19 ± 3.3	1.07 ± 0.21	1.4 ± 0.25	1.6 ± 0.26	1.15 ± 0.22	8
Wild Type (+)-CIQ	20 ± 1.8	20 ± 1.7	0.99 ± 0.03	1.2 ± 0.12	1.7 ± 0.11*	1.47 ± 0.10	17
GRIN2D-/- (+)-CIQ	24 ± 4.3	23 ± 5.3	0.95 ± 0.21	1.8 ± 0.17	1.6 ± 0.20	0.90 ± 0.20	4
Pyramidal							
Wild Type Vehicle	23 ± 2.6	19 ± 1.8	0.85 ± 0.16	2.5 ± 0.89	3.0 ± 1.0	1.33 ± 0.27	7
Wild Type (+)-CIQ	20 ± 1.6	19 ± 2.4	0.94 ± 0.15	2.9 ± 0.32	3.0 ± 0.29	1.09 ± 0.19	10

[a] AMPAR amplitudes were measured by the amplitude of fast component of the fitted composite mEPSC (mean ± SEM).
[b] NMDAR amplitudes were measured as the averaged response between 40-50 ms after the peak AMPAR response (mean ± SEM).
* $p<0.05$, Dunnett's test following a repeat measure ANOVA (Control vs Treatment).

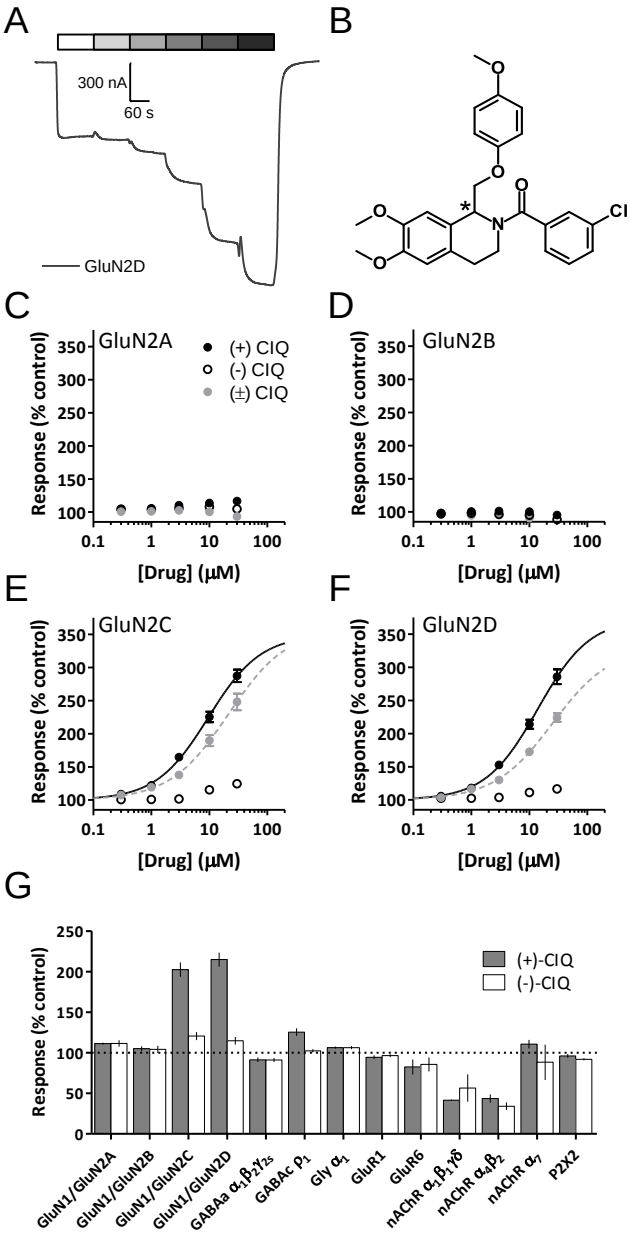
A
300 nA
60 s
GluN2D
B
O
O
O
O
*
N
Cl
C
GluN2A
(+) CIQ
(-) CIQ
(±) CIQ
Response (% control)
[Drug] (μM)
D
GluN2B
E
GluN2C
F
GluN2D
G
(+)-CIQ
(-)-CIQ
GluN1/GluN2A
GluN1/GluN2B
GluN1/GluN2C
GluN1/GluN2D
GABAa α1β2γ2s
GABAc ρ1
Gly α1
GluR1
GluR6
nAChR α1β1δ
nAChR α4β2
nAChR α7
P2X2

Figure 1

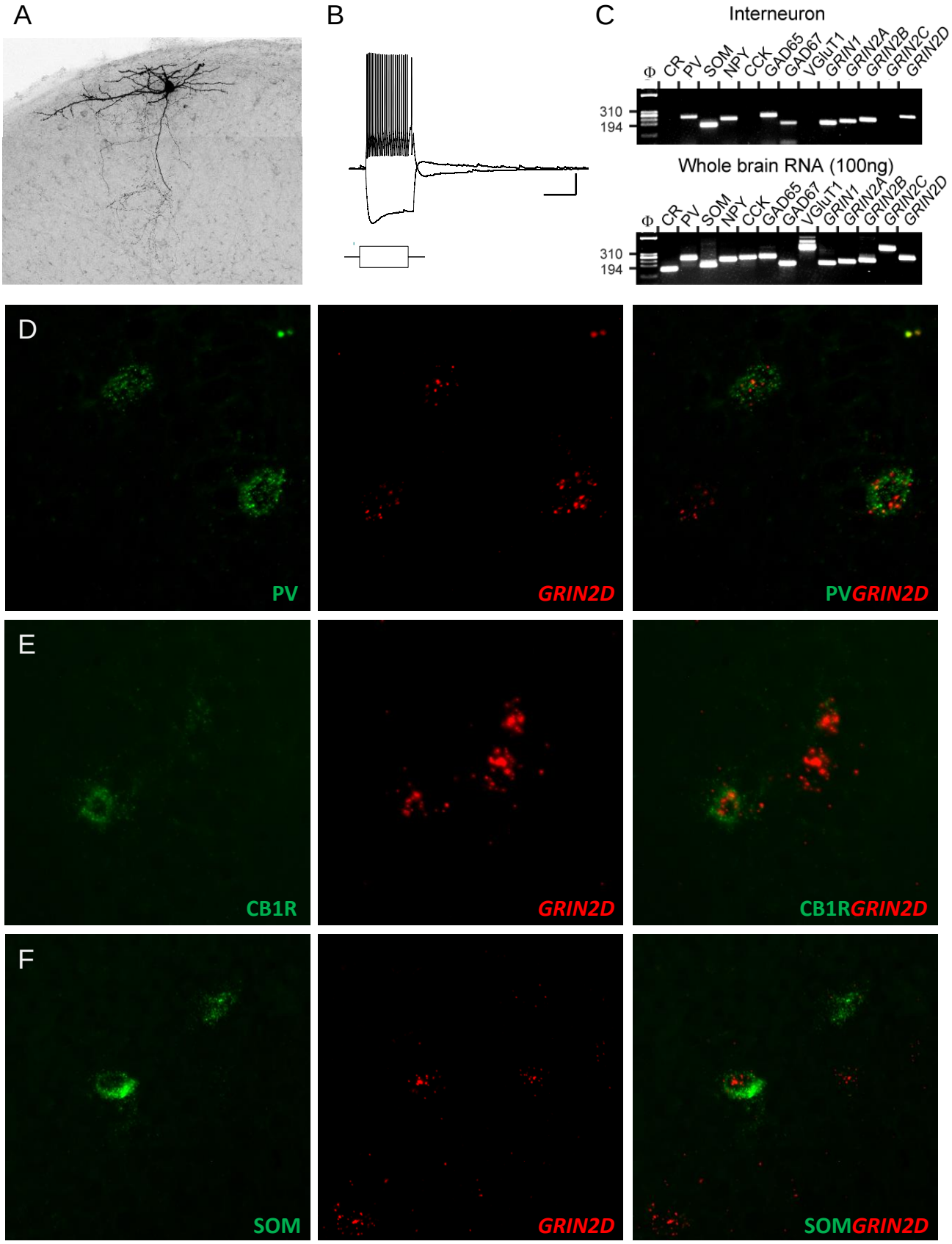
A
B
C
Interneuron
Φ CR PV SOM NPY CCK GAD65 GAD67 VGluT1 GRIN1 GRIN2A GRIN2B GRIN2C GRIN2D
310
194
Whole brain RNA (100ng)
Φ CR PV SOM NPY CCK GAD65 GAD67 VGluT1 GRIN1 GRIN2A GRIN2B GRIN2C GRIN2D
310
194
D
PV
GRIN2D
PVGRIN2D
E
CB1R
GRIN2D
CB1RGRIN2D
F
SOM
GRIN2D
SOMGRIN2D

Figure 2

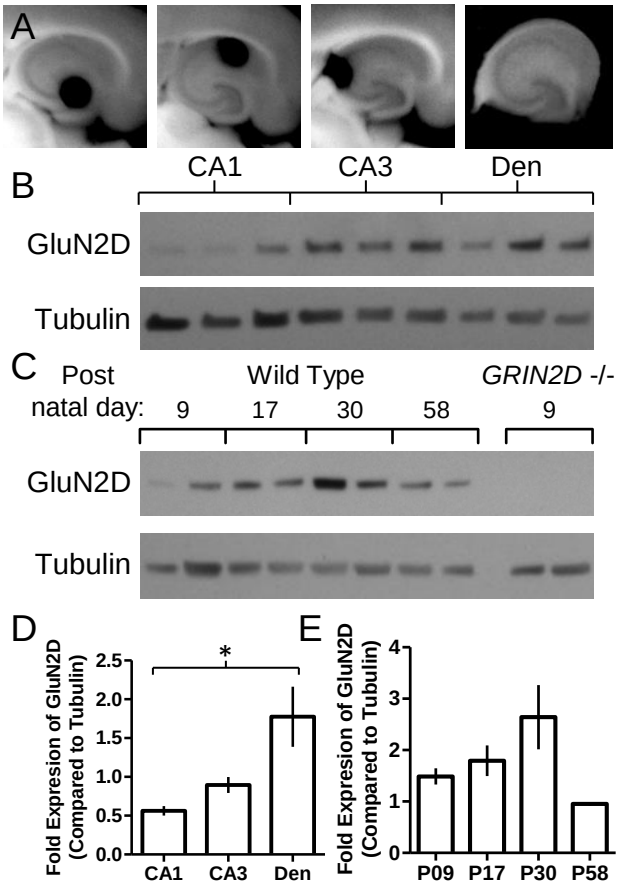
A
CA1
CA3
Den
B
GluN2D
Tubulin
C
Post
natal day:
Wild Type
9
17
30
58
GRIN2D -/-
9
GluN2D
Tubulin
D
Fold Expresion of GluN2D
(Compared to Tubulin)
2.5
2.0
1.5
1.0
0.5
0.0
*
CA1
CA3
Den
E
Fold Expresion of GluN2D
(Compared to Tubulin)
4
3
2
1
0
P09
P17
P30
P58

Figure 3

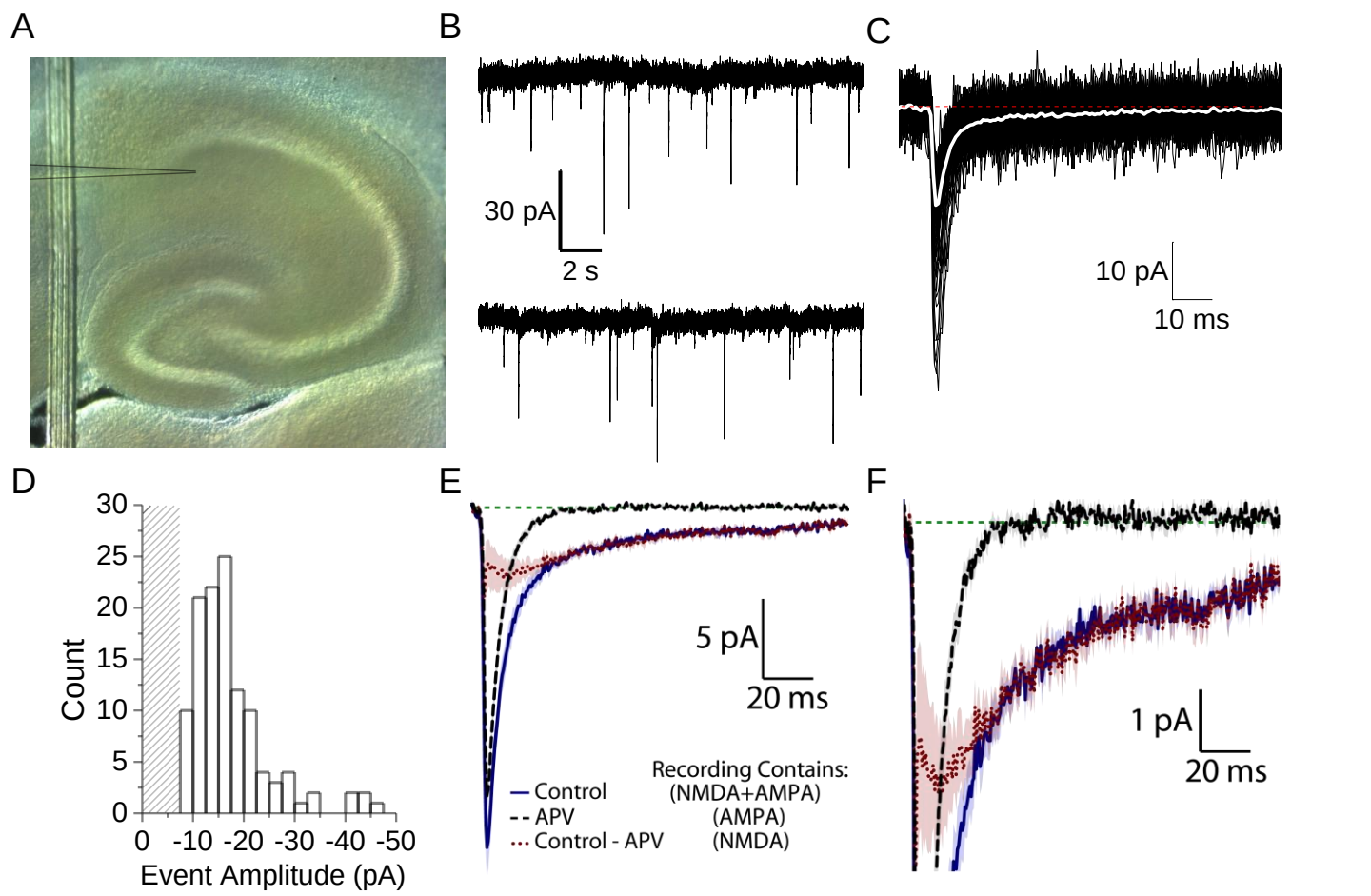
A
B
C
30 pA
2 s
10 pA
10 ms
D
E
F
Count
30
25
20
15
10
5
0
0 -10 -20 -30 -40 -50
Event Amplitude (pA)
5 pA
20 ms
Control
APV
Control - APV
Recording Contains:
(NMDA+AMPA)
(AMPA)
(NMDA)
1 pA
20 ms

Figure 4

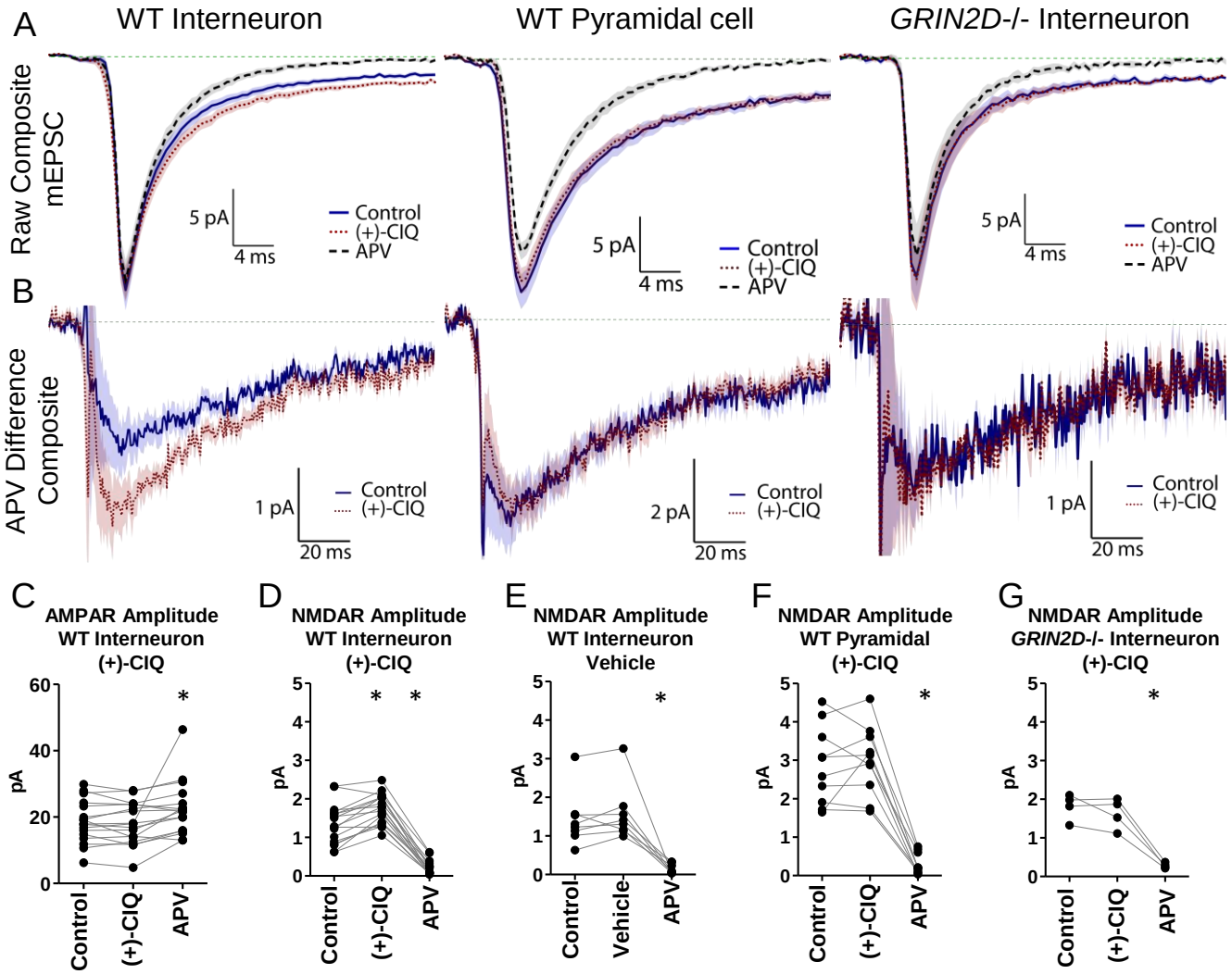
A
WT Interneuron
WT Pyramidal cell
GRIN2D-/- Interneuron
Raw Composite mEPSC
5 pA
4 ms
Control
(+)-CIQ
APV
B
APV Difference Composite
1 pA
20 ms
2 pA
C
AMPAR Amplitude
WT Interneuron
(+)-CIQ
pA
Control
(+)-CIQ
APV
D
NMDAR Amplitude
WT Interneuron
(+)-CIQ
E
NMDAR Amplitude
WT Interneuron
Vehicle
F
NMDAR Amplitude
WT Pyramidal
(+)-CIQ
G
NMDAR Amplitude
GRIN2D-/- Interneuron
(+)-CIQ

Figure 5

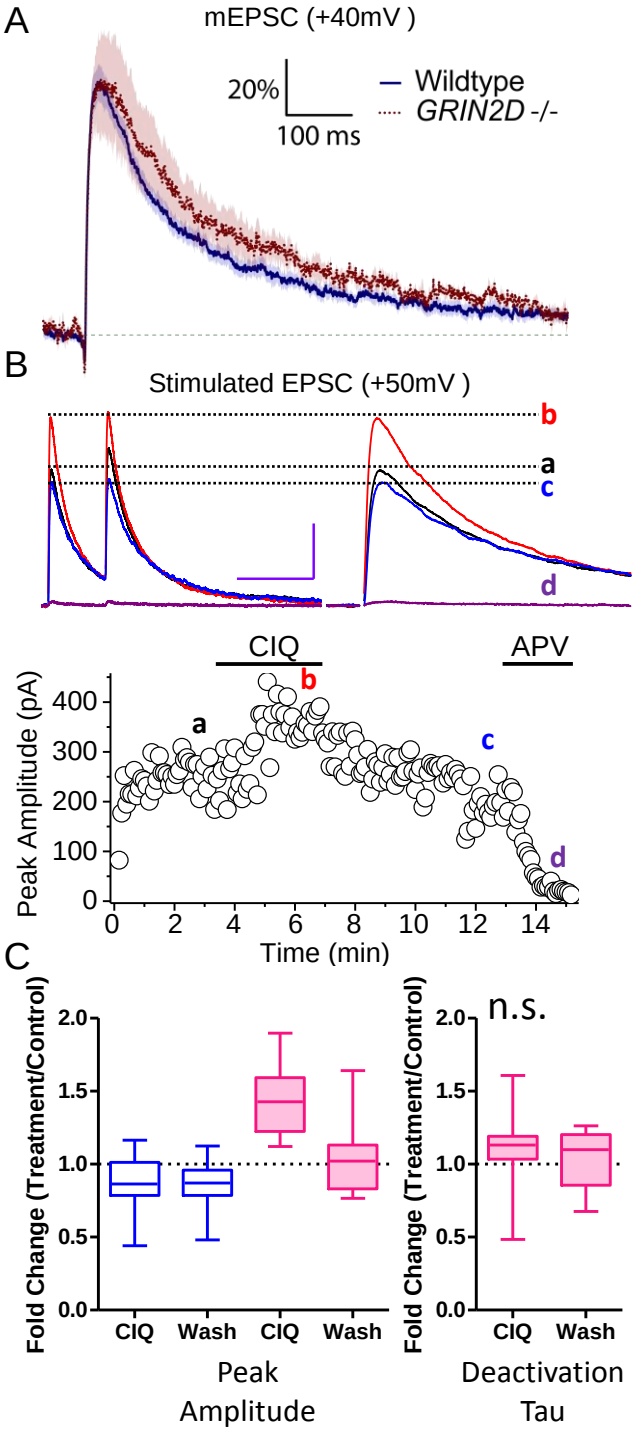
A
mEPSC (+40mV)
20%
100 ms
Wildtype
GRIN2D -/-
B
Stimulated EPSC (+50mV)
b
a
c
d
CIQ
APV
Peak Amplitude (pA)
400
300
200
100
0
0
2
4
6
8
10
12
14
Time (min)
C
Fold Change (Treatment/Control)
2.0
1.5
1.0
0.5
0.0
CIQ
Wash
CIQ
Wash
Peak
Amplitude
n.s.
Fold Change (Treatment/Control)
2.0
1.5
1.0
0.5
0.0
CIQ
Wash
Deactivation
Tau

Figure 6

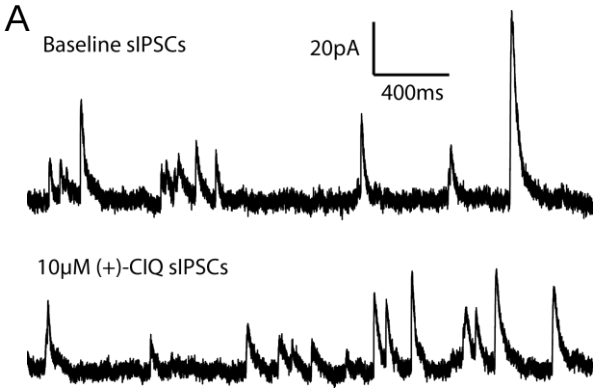
A
Baseline sIPSCs
20pA
400ms
10μM (+)-CIQ sIPSCs

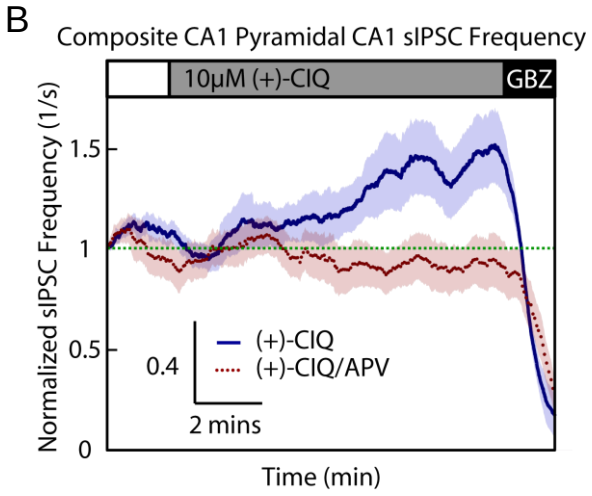
B
Composite CA1 Pyramidal CA1 sIPSC Frequency
10μM (+)-CIQ
GBZ
Normalized sIPSC Frequency (1/s)
1.5
1
0.5
0
0.4
2 mins
(+)-CIQ
(+)-CIQ/APV
Time (min)

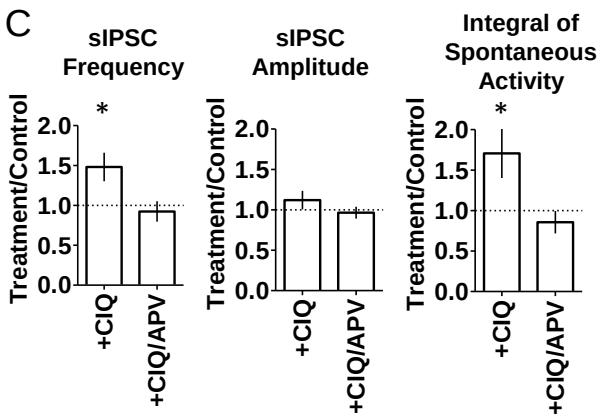
C
sIPSC Frequency
sIPSC Amplitude
Integral of Spontaneous Activity
Treatment/Control
2.0
1.5
1.0
0.5
0.0
*
+CIQ
+CIQ/APV

Figure 7